Evaluation of a Survivin-Based Recombinant Overlapping Peptide Vaccine Combined with FLASH Radiotherapy in the B16 Melanoma Model



Lianqing Chen

St Peter's College

Department of Oncology

University of Oxford

A thesis submitted for the degree of

MSc by Research in Oncology

Trinity 2026

Word count: 17520

Abstract

Building on the tumour-associated antigen survivin, our group previously developed a recombinant overlapping peptide-based human survivin vaccine (ROP-hSVN), which has advanced to clinical evaluation, although further strategies to enhance its antitumour efficacy are needed. Given a recent finding that higher survivin expression was associated with improved responses to ROP-SVN vaccination, radiation-induced upregulation of survivin provides a rationale for combining survivin-targeted vaccination with radiotherapy. FLASH radiotherapy may further enhance this strategy by inducing survivin upregulation while better preserving immune function. This study therefore evaluated the therapeutic potential of combining a ROP-based mouse survivin vaccine (ROP-mSVN) with FLASH radiotherapy.

To investigate this strategy, ROP-mSVN was successfully produced and purified, and the resulting vaccine induced detectable humoral and cellular immune responses in mice. Its therapeutic efficacy, alone and in combination with FLASH radiotherapy, was then evaluated in B16 melanoma-bearing mice. Notably, the combination treatment resulted in the lowest tumour burden among all treatment groups, although the difference between the combination treatment and ROP-mSVN vaccination alone did not reach statistical significance. Collectively, these findings suggest a potential benefit of combining ROP-mSVN vaccination with FLASH radiotherapy, but do not yet establish a definitive therapeutic advantage. Further studies with longer follow-up are needed to determine whether the combination can provide sustained tumour control.

Acknowledgements

I would like to express my sincere gratitude to my supervisors, Dr Shisong Jiang, Dr Kristoffer Petersson, and Dr Wenshu Lu, for their consistent guidance and support throughout my MRes research. I am grateful to all members of the Jiang Group for kindly sharing their knowledge and experience. I would especially like to thank Zachary Rawlinson for his generous support throughout my research, particularly for helping me settle into the lab and guiding me through the early stages of my work. I am also grateful to Han Hai for her encouragement and support whenever I encountered difficulties.

I am particularly thankful to Dr Salomé Paillas and Dr Jialing Ruan from the Petersson Group for their invaluable help in getting me started with the animal experiments and for their guidance throughout this part of the project. I would also like to thank Joanne Russell for her continued help throughout my time at Oxford.

Finally, I would like to thank my parents for their constant love and support throughout my studies abroad.

Declaration

I declare that the experimental results presented in this thesis are my own, except where otherwise stated. No part of this thesis has previously been submitted for any other degree at the University of Oxford or any other institution.

Lianqing Chen

August 2026

Table of Contents

Abstract I

Acknowledgements II

Declaration III

List of Abbreviations VIII

1 Introduction 1

1.1 Current cancer treatments 1

1.1.1 Surgery 1

1.1.2 Radiotherapy 3

1.1.3 Chemotherapy 5

1.1.4 Targeted therapy 6

1.1.5 Immunotherapy 8

Overview 8

Cancer vaccine 9

1.2 FLASH radiotherapy 12

1.2.1 Overview 12

1.2.2 Potential mechanisms 13

Oxygen depletion 14

Radical-radical recombination 15

Lipid peroxidation 15

Mitochondrial preservation 16

Immune preservation and modulation 17

1.2.3 Current clinical development 18

1.2.4 Challenges and future perspectives 19

1.3 Recombinant Overlapping Peptide (ROP)-based vaccines 21

1.3.1 Overview 21
1.3.2 Current clinical development 22
1.3.3 Challenges and future perspectives 25
1.4 Survivin 26
1.4.1 Biological functions 27
Regulation of apoptosis 27
Regulation of cell division 28
Other functions 29
1.4.2 Expression and clinical relevance in cancer 30
1.4.3 Survivin expression and radioresponse 31
1.4.4 Survivin expression and ROP-survivin vaccine response 33
1.5 Study rationale and aims 33
2 Method 37
2.1 Production of ROP-mSVN 37
2.1.1 cDNA Synthesis 37
2.1.2 Bacterial Transformation 37
2.1.3 Colony Screening 38
2.1.4 Protein Expression 38
2.1.5 Protein Purification 41
2.1.6 Protein Refolding 43
2.1.7 Protein Electrophoresis 44
2.1.8 Coomassie Protein Staining 44
2.1.9 Western Blot 44
2.1.10 Purity Assay 45
2.2 Evaluation of ROP-mSVN combined with FLASH radiotherapy 46
2.2.1 Licensing 46

2.2.2 Animals 46
2.2.3 Cell Culture and Maintenance 47
2.2.4 Immunofluorescence 47
2.2.5 Mycoplasma Test 49
2.2.6 Establishment of Tumour Models 50
2.2.7 FLASH Irradiation In Vivo 51
2.2.8 Vaccination 51
2.2.9 Serum Collection 52
2.2.10 ELISA 52
2.2.11 Isolation of Splenocytes 53
2.2.12 ELISpot 54
2.3 Data Analysis 55
3 Results 56
3.1 Production of ROP-mSVN 56
3.1.1 Recombinant ROP-mSVN protein expression 56
ROP-mSVN construct design 56
Investigation of conditions for ROP-mSVN expression 57
3.1.2 Recombinant ROP-mSVN protein purification 63
IMAC purification 63
Dialysis 67
3.1.3 Identity confirmation 68
3.1.4 Purity assessment 71
3.2 Evaluation of ROP-mSVN combined with FLASH radiotherapy 73
3.2.1 Immunogenicity evaluation of the ROP-mSVN vaccine 73
Experimental design 73
Humoral immune response 74

Cellular immune response 75
Vaccine tolerability 77
3.2.2 Establishment of the B16F10 melanoma model 78
Survivin expression in B16F10 cells 78
Mycoplasma testing 80
Characterisation of tumour growth 81
3.2.3 Therapeutic efficacy of ROP-mSVN vaccination combined with FLASH radiotherapy 82
Experimental design 83
Tumour growth following treatment 84
Endpoint tumour burden 86
4 Discussion 88
4.1 Production of the ROP-mSVN vaccine 88
4.2 Evaluation of ROP-mSVN combined with FLASH radiotherapy 92
4.3 Limitations and future directions 96
4.4 Conclusion 99
References 100

List of Abbreviations

Abbreviation	Full term
APC	Antigen-Presenting Cells
BIR	Baculovirus IAP Repeat
CIRT	carbon-ion radiotherapy
CONV-RT	Conventional Radiotherapy
CPC	Chromosomal Passenger Complex
EGFR	Epidermal Growth Factor Receptor
FDA	Food and Drug Administration
FLASH-RT	FLASH Radiotherapy
hSVN	Human Survivin
IAP	Inhibitor of Apoptosis Proteins
ICI	Immune Checkpoint Inhibitors
IMAC	Immobilised Metal Affinity Chromatography
IPTG	Isopropyl β-D-1-thiogalactopyranoside
LRMK	Leu-Arg-Met-Lys sequence
MHC	Major Histocompatibility Complex
MRD	Minimal Residual Disease
MRT	Microbeam Radiation Therapy
mAbs	Monoclonal antibodies
mSVN	Mouse Survivin
NES	Nuclear Export Signal
NSCLC	Non-Small Cell Lung Cancer
ROP	Recombinant Overlapping Peptide
ROS	Reactive Oxygen Species
SMKIs	Small-Molecule Kinase Inhibitors
SVN	Survivin
TAAs	Tumour-Associated Antigens
TSAs	Tumour-Specific Antigens
TME	Tumour Microenvironment
UHDR	Ultra-High-Dose-Rate

1 Introduction

1.1 Current cancer treatments

Cancer, characterized by uncontrolled cellular proliferation, remains a leading cause of death worldwide (Bray, Laversanne et al. 2024). Over the past decades, substantial efforts have been made to advancing cancer treatment. Starting with surgery, cancer treatment has evolved to include radiotherapy, chemotherapy, targeted therapy, and more recently immunotherapy and other emerging therapeutic strategies. An increasingly diverse range of treatment options has been developed to improve clinical outcomes through distinct mechanisms, although the challenges associated with cancer treatment are far from being fully resolved.

1.1.1 Surgery

Surgery is the oldest recognised treatment for cancer (Wyld, Audisio et al. 2015), and it remains a primary treatment for a wide range of solid tumours (Wagle, Nogueira et al. 2025). By removing the tumour together with a surrounding margin of healthy tissue, cancer surgery aims to completely clear the tumour cells (Wyld, Audisio et al. 2015). However, this goal is not always achievable. Minimal residual disease (MRD), defined as occult tumour cells that persist following surgical resection, has been widely reported (Coffey, Wang et al. 2003, Jacome and Johnson 2023). Importantly, surgical removal may contribute to the progression of MRD (Riggio, Varley et al. 2021). Accumulating evidence

also suggests that surgery may facilitate the establishment of new metastatic lesions (Tohme, Simmons et al. 2017).

Several interrelated mechanisms may link surgery to metastasis, including the induction of systemic stress and inflammation, immune suppression, microbiome dysbiosis, and enhanced release of circulating tumour cells (Nalisa, Luvhengo et al. 2026). Growing interest has focused on strategies to mitigate the pro-tumour effects of surgery. During surgery, potential approaches include localised delivery of immunomodulators (Chang, Shin et al. 2025, Xu, Zhang et al. 2025), intraoperative radiotherapy (Palavani, de Barros Oliveira et al. 2024, Tao, Zhang et al. 2024), and oncolytic viruses (Volovat, Scripcariu et al. 2024). Systemic measures may also involve pharmacological modulation of stress and inflammatory pathways, such as β-adrenergic inhibition and COX-2 blockade (Tan, Zhang et al. 2026). Particularly, neoadjuvant and adjuvant immunotherapies may further mitigate the risk of surgery-associated metastasis and recurrence by reversing immunosuppression and promoting sustained immune surveillance against residual and disseminated tumour cells (Tarhini, Eads et al. 2022, Parisi, Abdayem et al. 2024, Haanen, Schumacher et al. 2026, Tan, Zhang et al. 2026). However, the optimal timing and duration of these strategies remain to be established, and their efficacy may vary across tumour types (Tan, Zhang et al. 2026).

1.1.2 Radiotherapy

Radiotherapy is a cornerstone of current cancer treatment (Chandra, Keane et al. 2021). It aims to damage or control the growth of cancer cells, either by directly damaging their DNA or by indirect cellular damage associated with the production of free radicals (Gianfaldoni, Gianfaldoni et al. 2017). Multiple forms of radiation are used in radiotherapy, including X-rays, electrons, and protons (Vaidya 2024). While radiation is effective in killing cancer cells, unavoidable exposure of surrounding healthy tissues during treatment can result in acute and long-term adverse effects (Verginadis, Citrin et al. 2025).

Several strategies have been developed to reduce normal-tissue exposure and widen the therapeutic window of radiotherapy. Advances in treatment planning and image guidance, including intensity-modulated and adaptive radiotherapy, enable more conformal dose delivery and allow treatment to be adjusted according to anatomical changes during therapy, potentially reducing tissue toxicity (Verginadis, Citrin et al. 2025). Particle therapy provides an alternative approach to normal-tissue sparing. Proton therapy exploits the Bragg peak to reduce exit dose and integral radiation exposure, while carbon-ion radiotherapy (CIRT) combines a favourable dose distribution with the higher linear energy transfer and relative biological effectiveness of carbon ions, offering potential advantages in balancing tumour control with normal-tissue sparing (Ioakeim-Ioannidou, Rose et al. 2024, Kwong and Hassanzadeh 2026). Recently, FLASH radiotherapy has emerged as a potential strategy to further widen the therapeutic window by reducing normal-tissue

toxicity while maintaining tumour control, although its clinical efficacy and underlying mechanisms remain under investigation (Vozenin, Montay-Gruel et al. 2026).

Another main challenge of radiotherapy is radiation resistance (Akhunzianov, Rozhina et al. 2025). Various mechanisms contribute to radiation resistance, including DNA damage repair, evasion of apoptosis, and alterations in the tumour microenvironment, which ultimately lead to cancer metastasis and recurrence (Wu, Song et al. 2023).

To overcome radioresistance and improve the therapeutic efficacy of radiotherapy, several approaches have been investigated. Pharmacological radiosensitisers have been developed to enhance tumour sensitivity to irradiation through multiple mechanisms, including modulation of DNA damage repair, oxidative stress and tumour hypoxia (Chen, Yan et al. 2025). Molecularly targeted approaches have increasingly focused on the inhibition of DNA damage response (DDR), targeting DDR components such as ATM, ATR, DNA-PK, and PARP (Cheng, Ding et al. 2025). Despite the potential of these sensitising strategies in radiotherapy, the clinical application of these sensitising strategies remains challenging, including limited selectivity, undesirable toxicity to normal tissues (Cao, Deng et al. 2025), and compensatory activation of alternative pathways (Fu, Li et al. 2024).

Notably, beyond its direct cytotoxic effects, radiotherapy also modulates antitumour immunity through both immunostimulatory and immunosuppressive mechanisms. Radiation-induced tumour cell death has been shown to promote the release of tumour antigens and expression of MHC-I molecules on tumour cells, facilitating the recognition of tumour cells by cytotoxic T cells (Lynch, Pitroda et al. 2024). However, radiotherapy can also exert immunosuppressive effects, including lymphocyte depletion, T-cell exhaustion and remodelling of the tumour microenvironment towards an immunosuppressive state (Darragh and Karam 2026). Combinations of radiotherapy with immunotherapy has therefore emerged as a promising strategy to harness the immunostimulatory effects of radiotherapy while mitigating its immunosuppressive effects (Hartley, Ebert et al. 2025, Darragh and Karam 2026).

1.1.3 Chemotherapy

Chemotherapy represents another major pillar of cancer treatment (Anand, Dey et al. 2023). Notably, the detailed mechanisms underlying the cytotoxic effects of conventional chemotherapy agents remain incompletely understood (Letai and de The 2025). Generally, most of these chemotherapy agents induce cell death by targeting essential cellular processes, such as DNA replication, transcription, and mitotic progression (Zafar, Khatoon et al. 2025). Such mechanisms lack tumour selectivity and therefore also affect normal cells with high proliferative activity, leading to various adverse effects (Anand, Dey et al.

2023). Drug resistance is another major concern associated with chemotherapy (Gu, Yang et al. 2025). Chemoresistance can be either intrinsic, existing before treatment begins, or acquired, developing during therapy (Ramos, Sadeghi et al. 2021). General mechanisms of chemoresistance include drug efflux, altered drug metabolism, enhanced DNA repair, and apoptosis evasion (Gu, Yang et al. 2025).

To overcome chemotherapy resistance, strategies that optimize the delivery of chemotherapeutic agents emerged (Gu, Yang et al. 2025). For example, several nanoparticle-based drug delivery systems have been reported to reverse drug resistance by inhibiting efflux transporters and anti-apoptosis pathway (Yao, Zhou et al. 2020). Additionally, the combination of chemotherapy with other therapies, including radiotherapy, immunotherapy, and epigenetic drug, has been widely explored (Eslami, Memarsadeghi et al. 2024).

1.1.4 Targeted therapy

With an improved understanding of cancer biology, targeted therapies have been developed to target tumour-associated genetic alterations and signalling pathways (Lee, Tan et al. 2018). Targeted therapies mainly include monoclonal antibodies (mAbs) and small-molecule kinase inhibitors (SMKIs). mAbs target extracellular ligands and membrane proteins, such as vascular endothelial growth factor (VEGF) and epidermal

growth factor receptor (EGFR), while most SMKIs inhibit protein kinases related to the proliferation, survival, and transformation of cancer cells (Wang and Tang 2026). Many targeted therapies have been approved by the U.S. Food and Drug Administration (FDA) since the late 20th century, including targeted agents against human epidermal growth factor receptor 2 (HER2), EGFR, VEGF, and B-cell lymphoma 2 (Bcl-2) (Min, Lee et al. 2022).

Although targeted therapy is expected to exhibit fewer side effects than traditional chemotherapy due to its improved specificity, various adverse effects have been observed in patients receiving targeted therapy, ranging from asthenia to cardiotoxicity and bleeding (Smith and Prasad 2021). Notably, responses to targeted therapies vary significantly among patients with different genetic profiles. Primary resistance to targeted therapy is associated with cellular, genetic and epigenetic changes that prevent cancer cells from responding to initial therapy, while acquired resistance arises through multiple mechanisms, including secondary mutations in the targeted genes, overexpression of the target proteins, activation of alternative signalling pathway, and the expansion of pre-existing therapy-resistant cell populations under selective pressure (Min, Lee et al. 2022, Ou, Gao et al. 2024). Current efforts to overcome such resistance include the development of personalized targeted agents and the investigation of combination therapies with immune checkpoint inhibitors (Xiang, Liu et al. 2024).

1.1.5 Immunotherapy

Overview

Immunotherapy represents a transformative approach in the field of oncology (Waldman, Fritz et al. 2020). Rather than directly targeting tumour cells, cancer immunotherapy harnesses the immune system to recognize and eliminate cancer cells specifically (Zhang, Liu et al. 2025).

Immune checkpoint inhibitors (ICIs) are one of the most promising advances in cancer immunotherapy, blocking immune checkpoint proteins that suppress immune cell cytotoxicity (Mc Neil and Lee 2025). Several ICIs have been approved by FDA, including inhibitors of cytotoxic T-lymphocyte associated antigen 4 (CTLA-4), programmed death 1 (PD-1), programmed death-ligand 1 (PD-L1), and lymphocyte-activation gene 3 (LAG-3) (Mc Neil and Lee 2025). These ICIs have been used to treat more than 20 types of cancer, demonstrating impressive clinical success (Tan, Day et al. 2022). However, immune-related adverse events and treatment resistance remain major obstacles to ICI therapy (Mc Neil and Lee 2025).

Chimeric antigen receptor (CAR)-T cell therapy is a novel immunotherapy that has revolutionized the treatment of several hematologic malignancies (Zugasti, Espinosa-Aroca et al. 2025). This approach engineers T-cells to express chimeric antigen receptors, redirecting them to eliminate tumour cells that express specific antigens (Sadelain 2017).

Despite initial clinical success, CAR-T cell therapy continues to face several challenges, including antigen heterogeneity, off-target effects, cytokine release syndrome, insufficient infiltration, and the immunosuppressive tumour microenvironment (TME) (Luo and Zhang 2024, Zugasti, Espinosa-Aroca et al. 2025).

Beyond ICIs and CAR-T cell therapy, additional cancer immunotherapeutic approaches are being explored, including cancer vaccines (Khleif and Gupta 2025), oncolytic viruses (Xiao, Zhang et al. 2026), bispecific antibodies (Klein, Brinkmann et al. 2024).

Cancer vaccine

Cancer vaccines are designed to activate antitumour immunity in the host by delivering tumour antigens (Sellars, Wu et al. 2022). Prophylactic cancer vaccines aims to prevent cancer development in tumour-free individuals, while therapeutic cancer vaccines are intended to educate the immune system to eliminate established tumours (Pail, Lin et al. 2025).

The selection of target antigen is key to cancer vaccine design. Many early cancer vaccines targeted tumour-associated antigens (TAAs), which are overexpressed in tumour cells but also expressed at low levels in normal tissues (Yarchoan, Johnson III et al. 2017). However, various TAA-targeting vaccines have failed to demonstrate satisfactory efficacy in clinical trials, partly due to their poor immunogenicity (Tsujikawa, Crocenzi et al. 2020,

Haakensen, Öjlert et al. 2024, Zaidi, Jaffee et al. 2025). With advances in sequencing technologies and computational algorithms, an increasing number of vaccines have been developed to target tumour-specific antigens (TSAs), which arise during tumorigenesis and are completely absent from normal cells (Yarchoan, Johnson III et al. 2017). Compared to TAA-based vaccines, TSA-based vaccines have the potential to induce stronger immune response, as TSAs are more distinct from self-antigens and less affected by central tolerance mechanism (Zaidi, Jaffee et al. 2025). Nevertheless, the limited sharing of TSAs across tumours restricts their applicability as universal vaccine targets (Zhou, Wei et al. 2025).

Various delivery platforms have been developed for cancer vaccines. Peptide vaccines, incorporating tumour epitopes, have demonstrated favourable safety profiles in humans but are limited by HLA restrictions and poor immunogenicity (Zhou, Wei et al. 2025). Distinct from peptide vaccines, DNA- and RNA-based vaccines offer greater scalability and versatility, and they enable the encoding of multiple antigens and immunostimulatory molecules (Saxena, van der Burg et al. 2021, Zaidi, Jaffee et al. 2025). Despite these advantages, mRNA vaccines remain susceptible to degradation in vivo due to innate immune recognition (Huff, Jaffee et al. 2022), while DNA vaccines are constrained by limited immunogenicity (Shariati, Khezrpour et al. 2025).

Another type of cancer vaccine is the cell-based vaccine, which includes both engineered cancer cell lines and antigen loaded dendritic cells (Zaidi, Jaffee et al. 2025). Cancer cell-based vaccines enable the presentation of numerous tumour antigens naturally expressed by cancer cells (Pérez-Baños, Gleisner et al. 2023), while dendritic cells loaded with antigens can trigger the activation, proliferation and differentiation of naive T-cells (Wculek, Cueto et al. 2020). Sipuleucel-T, the first FDA-approved therapeutic cancer vaccine, is an autologous dendritic cell-based vaccine (Kantoff, Higano et al. 2010). However, the manufacturing of cell-based vaccines is technically demanding and costly, which limits their clinical application (Zaidi, Jaffee et al. 2025).

At present, several challenges remain in translating therapeutic cancer vaccines into effective clinical treatments. The selection of sufficiently antigens remains challenging, particularly for tumour-associated antigens derived from self-proteins, which may be subject to immune tolerance and consequently elicit suboptimal T-cell responses *(Markosyan)*. Moreover, vaccine-induced T-cell responses may be insufficient to achieve effective tumour control in the presence of an immunosuppressive tumour microenvironment, impaired antigen processing and presentation, and other mechanisms of tumour immune evasion (Pail, Lin et al. 2025, Markosyan and Vonderheide 2026). Translating these immune responses into durable clinical benefit also remains challenging, with vaccine platform and treatment timing potentially influencing therapeutic efficacy (Haanen, Schumacher et al. 2026). Future strategies may therefore focus on improving

antigen selection, overcoming immunosuppressive mechanisms within the tumour microenvironment, and combining cancer vaccines with complementary treatment modalities to enhance antitumour immunity (Pail, Lin et al. 2025, Haanen, Schumacher et al. 2026).

Overall, remarkable advances have been achieved in cancer treatment over the past decades, but current therapeutic approaches remain limited by various factors, including treatment-related toxicity and tumour resistance. For some emerging therapies, high costs and limited accessibility also constrain their broader application. Therefore, further optimisation of existing therapies and the development of novel therapies will be essential to improve clinical outcomes for cancer patients.

1.2 FLASH radiotherapy

1.2.1 Overview

Although conventional radiotherapy (CONV-RT) remains a major option in cancer therapy, its toxicity to surrounding normal tissues can result in various adverse effects and limit its therapeutic potential. FLASH radiotherapy (FLASH-RT), a novel radiotherapy approach defined by the delivery of ultra-high-dose-rate (UHDR) radiation, has been shown to reduce normal tissue toxicity while maintaining comparable tumour control (Vozenin,

Bourhis et al. 2022). This differential sparing of normal tissues compared with tumour tissues is named the “FLASH effect”.

Common radiation sources investigated in FLASH-RT include electrons (Giannini, Gadducci et al. 2024), protons (Nesteruk and Psoroulas 2021), and photons (Montay‐Gruel, Corde et al. 2022), each with distinct advantages and limitations (Di, Meng et al. 2026). Electron-based UHDR irradiation is relatively well established, but its clinical application is restricted by the limited penetration depth (Vozenin, Bourhis et al. 2022, Kim and Zou 2023). In contrast, proton FLASH-RT offers the potential for treating deep-seated tumours due to a physical property of protons known as the Bragg peak (Kim and Zou 2023). However, achieving proton-based UHDR remains technically challenging (Kim and Kim 2024). Finally, photon FLASH-RT remains difficult to implement and is still at an early stage of development (Di, Meng et al. 2026).

1.2.2 Potential mechanisms

Although the tissue-sparing effect of FLASH has been demonstrated in various preclinical models, the underlying mechanisms remain incompletely understood. Several hypotheses have been proposed to explain this phenomenon, including oxygen depletion, lipid peroxidation, radical-radical recombination, mitochondrial preservation, and immune cell preservation.

Oxygen depletion

Oxygen depletion is among the earliest mechanisms proposed to explain the FLASH effect, suggesting that FLASH-RT may protect normal tissues through rapid oxygen consumption during irradiation (Rosini, Ciarrocchi et al. 2025). FLASH-RT at ultra-high dose rates has been hypothesised to induce a transient reduction in oxygen availability in normal tissues, thereby attenuating the contribution of oxygen to radiation-induced DNA damage (Wilson, Hammond et al. 2020). In contrast, the prolonged delivery time of CONV-RT allows continuous oxygen replenishment during irradiation, potentially diminishing this protective effect (Rosini, Ciarrocchi et al. 2025). A recent study supports this hypothesis by demonstrating that the tissue-sparing effect of FLASH was observed in mice breathing normal air but was absent in pure oxygen-breathing mice (Zhang, Gerweck et al. 2023).

However, several studies have suggested that oxygen consumption during FLASH irradiation may be insufficient to produce hypoxia that could account for the observed tissue protection (Cao, Zhang et al. 2021, Jansen, Knoll et al. 2021, El Khatib, Van Slyke et al. 2022). Furthermore, an in vitro study reported lower oxygen consumption following FLASH-RT compared with CONV-RT (Cao, Zhang et al. 2021). Together, these findings highlight the need to explore additional mechanisms that may contribute to the FLASH effect.

Radical-radical recombination

A different hypothesis is that FLASH-RT induces a transiently high concentration of free radicals, which may promote radical recombination into non-radical species, thereby limiting subsequent oxidative damage (Labarbe, Hotoiu et al. 2020). Consistent with this concept, molecular simulations suggested that the high transient reactive oxygen species (ROS) density generated during FLASH irradiation facilitates ROS aggregation into less reactive forms (Abolfath, Grosshans et al. 2020). This effect is more pronounced under physioxic oxygen conditions than in hypoxic conditions but reaches a plateau at higher oxygen concentrations, which may contribute to the differential responses of normal and tumour tissues to FLASH irradiation (Abolfath, Grosshans et al. 2020).

Lipid peroxidation

Lipid peroxidation, a free radical-mediated process that can cause substantial cellular damage, has been associated with radiation-induced ferroptosis (Pearson, Carmicheal et al. 2021). Compared to CONV-RT, FLASH-RT generates reactive species at a much higher dose rate (Rosini, Ciarrocchi et al. 2025). It is therefore hypothesised that, in the context of FLASH-RT, normal cells are more efficient at limiting radiation-induced oxidative stress than tumour cells due to their greater antioxidant capacity, thereby limiting lipid peroxidation chain reactions and ultimately reducing toxicity (Spitz, Buettner et al. 2019, Geirnaert, Kerkhove et al. 2025, Rosini, Ciarrocchi et al. 2025). This protective advantage is less pronounced under CONV-RT, as the slower generation of free radicals allows

antioxidant systems in both normal and tumour cells to effectively neutralize them (Rosini, Ciarrocchi et al. 2025). Recent work has provided further mechanistic insights into such differential effects of FLASH-RT (Vilaplana-Lopera, Kim et al. 2025). A high-iron diet abrogated the protective effects of FLASH-RT on normal tissue, suggesting that differences in baseline iron levels between normal and cancerous tissues may play an important role in mediating this differential response.

Mitochondrial preservation

Under normal conditions, mitochondria are efficient in removing excessive ROS and repairing oxidative damage through their antioxidant system (Napolitano, Fasciolo et al. 2021). However, the substantial ROS production induced by radiotherapy could overwhelm this antioxidant system, leading to mitochondrial damage and ultimately cellular dysfunction (Rosini, Ciarrocchi et al. 2025). It has been shown that FLASH-RT attenuated mitochondrial damage in normal lung fibroblasts compared with CONV-RT, as reflected by both morphological and functional alterations, suggesting that mitochondrial preservation may contribute to the FLASH effect (Guo, Buonanno et al. 2022). Recent proteomic analysis further demonstrated that, compared with CONV-RT, FLASH-RT results in reduced damage to proteins involved in mitochondrial function, including those associated with oxidative phosphorylation (Ren, Hou et al. 2024). Further research is required to elucidate the mechanisms underlying this mitochondrial-sparing effect of FLASH.

Immune preservation and modulation

The ultrahigh dose rate of FLASH-RT enables the prescribed dose to be delivered over a much shorter timescale. It has therefore been suggested that this shorter irradiation time may result in a smaller fraction of circulating immune cells being exposed to radiation, potentially preserving immune function (Durante, Bräuer-Krisch et al. 2018). This immune-sparing effect of FLASH-RT has been demonstrated in a computational model, where the killing of circulating immune cells was significantly reduced at ultra-high dose rates compared with conventional dose rates (Jin, Gu et al. 2020). Several studies have provided further evidence supporting this hypothesis. In a murine orthotopic lung tumour model, FLASH-RT has been shown to enhance T lymphocyte infiltration into the tumour microenvironment compared with CONV-RT (Rama, Saha et al. 2019). Additionally, in tumour-bearing mice, a higher proportion of CD8+ T cells in the spleen was observed after FLASH-RT than after CONV-RT (Zhu, Xie et al. 2023).

Beyond lymphocyte preservation, emerging evidence suggests that FLASH-RT may also modulate the tumour immune microenvironment. For example, in a murine medulloblastoma model, FLASH-RT promoted a more pro-inflammatory macrophage phenotype, reduced immunosuppressive macrophage polarisation and increased T-cell infiltration compared with CONV-RT (Ni, Reitman et al. 2025).

Notably, several studies have shown that FLASH-RT exhibits comparable rather than enhanced antitumour efficacy compared with CONV-RT in multiple murine tumour models, including lung, glioblastoma, and ovarian (Kim, Gwak et al. 2021, Montay-Gruel, Acharya et al. 2021, Eggold, Chow et al. 2022). Therefore, the full impact of FLASH-RT on antitumor immunity remains to be further elucidated.

1.2.3 Current clinical development

The first-in-human treatment with FLASH-RT was reported in a patient with cutaneous lymphoma in 2019 (Bourhis, Sozzi et al. 2019). The patient received a single dose of 15 Gy electron FLASH-RT, and a durable tumour response was observed during the 5-month follow-up period. This study provided preliminary evidence that FLASH-RT is technically feasible for clinical application and does not cause unacceptable toxicity. However, the findings were limited by the sample size (n=1). Additionally, only a superficial skin tumour was treated, leaving the clinical applicability of FLASH-RT for deeper-seated malignancies uncertain (Di, Meng et al. 2026).

Further evidence on the feasibility and safety of FLASH-RT was provided by a nonrandomized trial in 2022 (Mascia, Daugherty et al. 2023). 8 Gy of FLASH-RT was given to 10 patients with bone metastases. Complete response was reported in 50% patients, and adverse events were comparable to those observed following conventional

radiotherapy. This study also represented the first-in-human clinical evaluation of proton FLASH-RT. However, the relatively short follow-up period limited the assessment of potential late toxicities (Di, Meng et al. 2026). Several clinical trials are currently evaluating the safety, feasibility and efficacy of FLASH-RT across different tumour types, including thoracic bone metastases, melanoma skin metastases, and non-melanoma skin cancers (NCT05524064; NCT04986696; NCT06549439; NCT05724875).

1.2.4 Challenges and future perspectives

Despite the promising preclinical evidence supporting the application of FLASH-RT in cancer treatment, the exact mechanisms underlying the FLASH effect remain a topic of ongoing debate. A clearer understanding of these mechanisms is essential for the safe and reliable clinical translation of FLASH-RT (Di, Meng et al. 2026), and multidisciplinary efforts integrating radiobiology, physics, chemistry, and engineering will be needed to achieve this (Vozenin, Montay-Gruel et al. 2026). In addition, larger-scale clinical studies are needed to establish the therapeutic window for FLASH-RT, which may vary among different tissues (Di, Meng et al. 2026). Defining dose-rate thresholds for individual tissue types will be essential to maximise the therapeutic benefits while maintaining treatment safety (Vozenin, Montay-Gruel et al. 2026). Notably, internationally standardised dosimetry protocols for ultra-high-dose-rate irradiation are lacking, which restricts the comparability of findings across institutions and complicates multicentre clinical trials (Di,

Meng et al. 2026). Future efforts are needed to enable more comprehensive clinical evaluation and facilitate the clinical translation of FLASH-RT.

To expand the therapeutic potential of FLASH-RT, the combination of FLASH-RT with other cancer therapies, including immunotherapy, has attracted growing interest (Rosini, Ciarrocchi et al. 2025). FLASH irradiation has been demonstrated to improve the antitumour efficacy of anti-PD-1 therapy (Eggold, Chow et al. 2022). Compared with CONV-RT, several studies have reported that FLASH-RT provides multiple immune benefits, including improved intratumoral T-cell infiltration and reduced deleterious immune responses in normal tissues (Eggold, Chow et al. 2022, Shi, Yang et al. 2022). More recently, FLASH-RT has been shown to stimulate pro-inflammatory polarisation of tumour macrophages and sensitise CAR-T cell therapy in a medulloblastoma model (Ni, Reitman et al. 2025), further highlighting its potential for combination with immunotherapy to modulate tumour immunosuppression. Further investigation into the therapeutic effects of FLASH-RT in combination with a broader range of anticancer therapies would be valuable.

1.3 Recombinant Overlapping Peptide (ROP)-based vaccines

1.3.1 Overview

As discussed in Section 1.1.5, cancer vaccines represent a promising immunotherapeutic strategy to activate antitumor immunity through various delivery platforms, including peptide-, DNA-, RNA-, and cell-based vaccines, each with distinct advantages and limitations. A main challenge of peptide-based vaccines is major histocompatibility complex (MHC) restriction (Shah, Holden et al. 2025), whereby a specific peptide epitope can only be presented by particular MHC molecules for T-cell recognition (Oyarzun and Kobe 2015). Additionally, peptide vaccines targeting TAAs often exhibit suboptimal immunogenicity due to immune tolerance, thereby limiting their clinical potential (Liu, Wu et al. 2024). To overcome these limitations, our group has developed a recombinant overlapping peptide (ROP)-based vaccine platform, which rearranges full-length antigens into a series of overlapping peptides connected by cleavable linkers (Jiang, Song et al. 2006, Zhang, Zhou et al. 2023).

In the ROP vaccine platform, the wide-type antigen sequence is divided into a series of 35-amino-acid-long peptide fragments, with a 10-amino-acid overlap between adjacent peptides (Zhang, Zhou et al. 2023). A Leu-Arg-Met-Lys (LRMK) sequence is incorporated between neighbouring peptide fragments, which could be recognised and cleaved by the cysteine protease Cathepsin S (Kallinteris, Wu et al. 2005, Xu, Lu et al. 2009). Cathepsin S is a key lysosomal protease involved in antigen processing, particularly in MHC class

II-mediated antigen presentation and MHC class I-mediated cross-presentation (Geetha and Skaria 2025). The incorporation of Cathepsin S-cleavable linkers therefore enables efficient processing of the ROP construct within antigen-presenting cells (APCs), generating a pool of overlapping peptides that can subsequently be loaded onto MHC molecules for T-cell activation (Zhang, Zhou et al. 2023). Compared with native proteins, ROPs have demonstrated several advantages, including enhanced immunogenicity, improved activation of both CD4+ and CD8+ T-cell responses (Cai, Zhang et al. 2017), and broader MHC epitope coverage (Zhang, Zhou et al. 2023). Furthermore, the absence of the native conformational structure of tumour antigen in ROPs may reduce potential oncogenic risks associated with the expression of intact oncoproteins (Zhang, Zhou et al. 2023).

Overall, the ROP technology provides a promising strategy to transform native TAAs into safer and more immunogenic vaccine candidates, with the potential to enhance the therapeutic efficacy of cancer vaccines.

1.3.2 Current clinical development

The ROP vaccine platform entered clinical evaluation for the first time with OVM-200, a survivin-based ROP (ROP-SVN) vaccine (Wijaya, Morris et al. 2026). Survivin is a tumour associated antigen that is overexpressed in the majority of human cancers (Chen,

Duan et al. 2016, Garg, Suri et al. 2016, Li, Lu et al. 2021), and its biological functions will be discussed further in Section 1.4.1. Preclinical studies demonstrated that ROP-SVN protein significantly prolonged survival in tumour-bearing mice compared with wide-type survivin protein (Cai, Zhang et al. 2017, Zhang, Zhou et al. 2023), supporting its therapeutic potential.

Between 2021 and 2023, a multicentre, open-label phase 1a trial evaluated the safety, tolerability and immunogenicity of the ROP-SVN vaccine in 12 patients with advanced ovarian cancer, prostate cancer or non-small cell lung cancer (NSCLC), who had exhausted standard treatment options (Wijaya, Morris et al. 2026). Patients received three doses of ROP-SVN vaccine at escalating dose levels. No treatment-related serious adverse events or dose-limiting toxicities were observed during the 6-month follow-up period. Among the dose cohorts, the highest dose (2000 μg) elicited the strongest humoral response, with antibody titres continuing to increase throughout follow-up. Consequently, the 2000 μg dose was selected for further evaluation in the phase 1b trial. Notably, robust survivin-specific T-cell responses were detected on Days 22 and 36 after the first vaccination but were not maintained until the end of follow-up. This transient response may reflect the natural contraction of vaccine-induced effector T cells following initial activation, together with limited persistence of the response in patients with advanced cancer. Collectively, these findings provide initial clinical evidence that the ROP-SVN vaccine can induce

potent cellular immunity even in patients with advanced stage IV cancers, while also indicating that sustaining long-term T-cell responses remains a challenge.

Building on the promising safety profile and immunogenicity observed in the phase 1a study, a phase 1b trial subsequently evaluated an extended immunisation regimen consisting of 3–11 doses of 2000 μg ROP-SVN vaccine (Jiang, Morris et al. 2026). Twenty-four patients with advanced ovarian, prostate cancer or NSCLC were enrolled. The vaccine again demonstrated a favourable safety profile and induced robust survivin-specific immune responses. Importantly, T-cell responses peaked on Day 57 after the first vaccination and remained significantly above baseline throughout the 6-month follow-up, suggesting that repeated antigen exposure through an extended immunisation regimen may support continued expansion and maintenance of vaccine-induced T-cell responses and thereby improve the durability of cellular immunity.

Notably, patient enrolment in the phase 1 studies was not restricted by specific HLA haplotypes (Wijaya, Morris et al. 2026). The robust humoral and cellular immune responses observed across this heterogeneous patient population provide preliminary clinical evidence that the ROP vaccine platform may overcome the HLA restriction that limits conventional peptide vaccines.

Beyond survivin, the ROP platform has also been applied to other tumour antigens, including the HPV oncogenic protein E7, although these applications remain at an early stage of development.

1.3.3 Challenges and future perspectives

Although promising safety and immunogenicity results of ROP-SVN have been reported in the phase 1 study, several limitations remain, including the small sample size (36 patients), limited tumour types, and relatively short follow-up period (Wijaya, Morris et al. 2026). Further clinical evaluation is required to comprehensively assess its therapeutic efficacy, long-term clinical benefit, and applicability across broader cancer populations.

As demonstrated in preclinical studies, although ROP-SVN vaccination induced robust immune responses and improved survival in tumour-bearing mice, its therapeutic efficacy as a monotherapy remained limited, with insufficient tumour regression observed (Zhang, Zhou et al. 2023). This limitation is commonly observed in cancer vaccines and may result from multiple factors, including the immunosuppressive tumour microenvironment and upregulation of inhibitory immune checkpoints, which promote T-cell exhaustion (Zhou, Wei et al. 2025). Therefore, exploring combination strategies with other anticancer therapies may help maximise the therapeutic potential of ROP-SVN vaccine. The combination of ROP-SVN vaccine with an anti-4-1BB agonistic antibody has been shown

to enhance antitumor efficacy in a B16F10 melanoma model compared with either monotherapy alone (Zhang, Zhou et al. 2023). Ongoing studies are further investigating the therapeutic potential of ROP-SVN vaccine in combination with other cancer treatments, including the FLASH radiotherapy strategy evaluated in the present study.

Beyond combination approaches, another promising direction is the translation of the ROP platform into the mRNA vaccine field. The development of mRNA-based ROP vaccines may provide advantages in terms of simplified manufacturing and broader applicability, further expanding the potential of this platform for cancer immunotherapy.

1.4 Survivin

Survivin, also known as BIRC5, is overexpressed in most human cancers, while its expression is undetectable in most adult normal tissues (Siragusa, Tomasello et al. 2024). It plays key roles in several cellular processes, including the regulation of apoptosis and cell division (Wang and Greene 2024). Survivin has long been considered a radioresistance factor (Chakravarti, Zhai et al. 2004), while our recent study also found that its expression was associated with tumour response to the ROP-based vaccine targeting survivin (Zhang, Zhou et al. 2023).

1.4.1 Biological functions

The functions of survivin are closely associated with its subcellular localisation. In the cytoplasm, survivin primarily acts as an inhibitor of apoptosis, while in the nucleus, it contributes to the regulation of cell division (Siragusa, Tomasello et al. 2024). A nuclear export signal (NES) plays a key role in the shift in the translocation of survivin from the nucleus to the cytoplasm (Stauber, Rabenhorst et al. 2006). Mutations in the NES have been shown to impair the anti-apoptotic function of survivin (Colnaghi, Connell et al. 2006). Beyond its roles in apoptosis and mitosis, survivin also participates in other cellular processes, including mitochondrial function (Townley and Wheatley 2020).

Regulation of apoptosis

As a member of the Inhibitors of Apoptosis protein (IAP) family, survivin has a Baculovirus IAP Repeat (BIR) domain (Srinivasula and Ashwell 2008). The BIR domain plays a key role in the interaction of survivin with other proteins containing IAP-binding motif, including apoptotic effectors Smac/DIABLO (Du, Kelly et al. 2012). It was extensively reported that overexpressing survivin in cells can induce anti-apoptotic protection while the ablation of survivin leads to enhanced apoptosis (Li, Ambrosini et al. 1998, Wheatley and Altieri 2019).

Survivin has been demonstrated to exert anti-apoptotic effects through both caspase-dependent and caspase-independent pathways (Siragusa, Tomasello et al. 2024). Unlike another IAP family member, XIAP, which inhibits caspase activity through directly binding to caspases (Huang, Park et al. 2001), survivin modulates the caspase-dependent apoptotic pathway, in part, by enhancing the anti-apoptotic activity of other IAP family members (Verhagen, Coulson et al. 2001). One proposed mechanism underlying this effect is the binding of survivin to Smac/DIABLO (Song, Yao et al. 2003, Du, Kelly et al. 2012), a mitochondrial protein that antagonises the activity of other IAP family members (Du, Fang et al. 2000, Verhagen, Ekert et al. 2000). Additionally, survivin has been suggested to suppress the activity of apoptosis-inducing factor, which mediates apoptosis through a caspase-independent mechanism (Pavlyukov, Antipova et al. 2011).

Regulation of cell division

Various cell cycle-dependent elements and cell cycle homology region boxes have been identified in the promoter sequence of survivin, suggesting a link between survivin and cell cycle regulation (Li, Ambrosini et al. 1998, LI and ALTIERI 1999). Indeed, survivin plays an essential role in cell division, and disruption of its function can result in defects in mitotic progression (Li, Ackermann et al. 1999, Lens, Wolthuis et al. 2003).

When localized in the nuclear, survivin is associated with the organization of the Chromosomal Passenger Complex (CPC), which plays a key role in mitosis (Vader, Kauw

et al. 2005, Carmena, Wheelock et al. 2012). The BIR domain of survivin interacts with phosphorylated histone H3 to facilitate the recruitment of other CPC proteins to the inner centromere (Kelly, Ghenoiu et al. 2010, Wiedemuth, Klink et al. 2014). During mitosis, survivin, together with other CPC proteins, contributes to proper chromosome alignment (Bolton, Lan et al. 2002). Previous studies have shown that survivin ablation leads to centrosomal defects and activation of a p53-dependent mitotic checkpoint (Beltrami, Plescia et al. 2004, Yang, Welm et al. 2004).

Notably, in physiological contexts such as in adult stem cells, survivin expression is tightly regulated throughout the cell cycle, while in cancer cells, survivin expression is markedly higher during G2/M but substantially lower during G1, indicating an aberrant cell cycle-dependent expression pattern (Xu, Fang et al. 2004, Siragusa, Tomasello et al. 2024).

Other functions

Survivin has been detected in the mitochondria of various tumour cell lines, while such mitochondrial localisation is absent in normal cells (Dohi, Beltrami et al. 2004, Townley and Wheatley 2020), suggesting a tumour-associated mitochondrial function of survivin. A mitochondrial targeting sequence has been identified at the N-terminus of survivin, which directs survivin to the mitochondria through interactions with translocase complexes in the mitochondrial membrane (Dunajová, Cash et al. 2016). Previous studies have demonstrated that mitochondrial survivin promotes tumour invasion by facilitating

mitochondrial trafficking to the cytoskeleton, thereby enhancing focal adhesion complex turnover (Rivadeneira, Caino et al. 2015). More recently, mitochondrial survivin was reported to suppress oxidative phosphorylation and increase glycolysis, which may support cancer cell survival by promoting a metabolic shift towards the Warburg effect (Townley and Wheatley 2020).

Beyond its cytoplasmic and nuclear localisation, survivin has also been detected in exosomes released by cancer cells (Khan, Jutzy et al. 2011, Galbo Jr, Ciesielski et al. 2017). Exosomal survivin has been implicated in cell–cell communication and may promote the proliferation and aggressive phenotype of neighbouring cancer cells (Khan, Jutzy et al. 2011).

1.4.2 Expression and clinical relevance in cancer

As a tumour-associated antigen, Survivin is overexpressed in tumour cells while its expression is undetectable in most adult tissues except stem cells (Siragusa, Tomasello et al. 2024). Survivin overexpression cover most cancers (Wang and Greene 2024), including melanoma (McKenzie, Liu et al. 2013), lung cancer (Falleni, Pellegrini et al. 2003), prostate cancer (Zhang, Coen et al. 2010), ovarian cancer (Nan, Gong et al. 2019), breast cancer (Knight, Oprea-Ilies et al. 2011), glioma (Zhang, Zhang et al. 2018), and haematological cancers (Small, Keerthivasan et al. 2010).

Survivin is associated with poor prognosis of cancers (Li, Lu et al. 2021). Prognostic value of survivin has been showed in various human cancer, including breast cancer (Veiga, Silva et al. 2019), head and neck squamous cell carcinoma (Zhou, Hu et al. 2021), non-small cell lung cancer (Zhang, Wang et al. 2012), gastric cancer (Liu, Gao et al. 2013). Notably, survivin-expressing circulating tumour cells has been detected in patients with various cancer types, which is associated with cancer metastasis and recurrence (Ning, Hanna et al. 2015, Qiao, Li et al. 2017, Warrier, Agarwal et al. 2020).

1.4.3 Survivin expression and radioresponse

Survivin has long been recognised as a radioresistance factor that enhances the radiation resistance of various human tumour cells (Chakravarti, Zhai et al. 2004, Rödel, Hoffmann et al. 2005, Pennati, Folini et al. 2008). High levels of survivin expression are associated with poor prognosis following radiotherapy (Rodel, Sprenger et al. 2012). It is commonly thought that survivin promotes radioresistance by inhibiting caspase-mediated apoptotic pathways (Akhunzianov, Rozhina et al. 2025). Accordingly, targeting survivin has been shown to sensitise cancer cells to radiotherapy (Li, Wang et al. 2017, Zhou, Guo et al. 2020).

Survivin expression has also been shown to increase following radiation, which may further enhance the resistance of tumour cells to subsequent irradiation (Grdina, Murley et

al. 2013). This radiation-induced upregulation of survivin has been suggested to be regulated by the transcription factor NF-κB (Grdina, Murley et al. 2013). Indeed, NF-κB-mediated induction of survivin following radiation has been observed in radioresistant cells but not in radiosensitive cells (Park, Yoon et al. 2016).

Notably, we previously observed a similar upregulation of survivin following FLASH irradiation, suggesting that radiation-induced survivin upregulation may represent a shared response to conventional and FLASH radiation (Haylene Lim and Zachary Rawlinson, unpublished data; **Figure 1**). Interestingly, we also observed a subsequent decrease in survivin expression at 48 h following both conventional and FLASH irradiation, which may be related to an increased proportion of apoptotic cells collected at this time point, as apoptotic cells have been reported to exhibit lower survivin expression (Terasaki, Terasaki et al. 2013). However, this possibility requires further investigation.

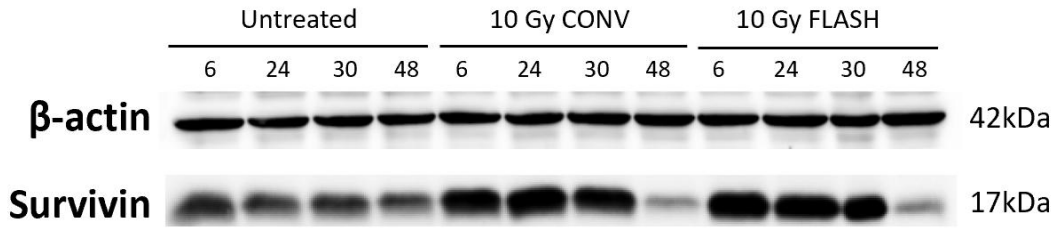


Figure 1. Survivin expression following conventional and FLASH irradiation. *HCT116 cells were left untreated, irradiated with 10 Gy conventional radiation (CONV), or 10 Gy FLASH radiation. Survivin expression was assessed by Western blotting at 6, 24, 30 and 48 h after*

irradiation. Both CONV-RT and FLASH irradiation induced survivin upregulation at 6, 24 and 30 h compared with untreated cells. β-actin was used as a loading control.

1.4.4 Survivin expression and ROP-survivin vaccine response

As discussed in Section 1.3.2, survivin is the target antigen of the first ROP-based vaccine to enter clinical evaluation (Wijaya, Morris et al. 2026). Survivin expression has been associated with tumour response to the ROP-SVN vaccine (Zhang, Zhou et al. 2023). In a murine melanoma model, tumour-bearing mice received ROP-SVN treatment, and survivin expression in the excised tumours was quantified using a double-antibody sandwich enzyme-linked immunosorbent assay (DAS-ELISA). Among tumours collected at the end of the ROP-SVN treatment, those with smaller volumes exhibited significantly higher survivin expression than those with larger volumes. It was proposed that higher survivin expression may enhance tumour visibility to the immune system activated by ROP-SVN. This also raises the possibility that ROP-SVN treatment may impose selection pressure on tumour cells, favouring the expansion of tumour cell populations with lower survivin expression and potentially contributing to vaccine resistance.

1.5 Study rationale and aims

Survivin (BIRC5) is a tumour-associated antigen overexpressed in most human cancers while showing limited expression in normal tissues (Section 1.4.2). Our group previously

developed a recombinant overlapping peptide (ROP)-human survivin (hSVN) vaccine that has advanced to clinical evaluation. However, its therapeutic efficacy as a monotherapy remained limited, with insufficient tumour regression observed, highlighting the need for strategies to further enhance its antitumour efficacy (Section 1.3).

Given a recent finding that higher survivin expression was associated with improved responses to ROP-SVN vaccination (Section 1.4.4), radiation-induced upregulation of survivin provides a basis for combining survivin-targeted vaccination with radiotherapy (Section 1.4.3). Additionally, radiation-induced enhancement of MHC class I expression and tumour antigen presentation may further facilitate the recognition of survivin-expressing tumour cells by vaccine-induced T cells (Section 1.1.3), offering a further rationale for the combination.

However, radiotherapy may also exert immunosuppressive effects, including lymphocyte depletion and remodelling of the tumour microenvironment towards an immunosuppressive state (Section 1.1.3), which may limit the potential benefits of combined therapy. FLASH radiotherapy has emerged as a novel radiotherapy approach that may better preserve immune function while maintaining tumour control (Section 1.2). Notably, we previously observed a similar upregulation of survivin following FLASH irradiation to that observed following conventional radiotherapy (**Figure 1**). This suggests that FLASH radiotherapy may retain the potential benefit of radiation-induced survivin

upregulation while potentially reducing the immunosuppressive effects associated with conventional radiotherapy, supporting its combination with ROP-SVN vaccination.

Together, these observations provide a rationale for combining ROP-mSVN vaccination with FLASH radiotherapy (**Figure 2**). This study therefore aimed to evaluate the antitumour efficacy of this combination and investigate whether the two treatments could achieve enhanced tumour control.

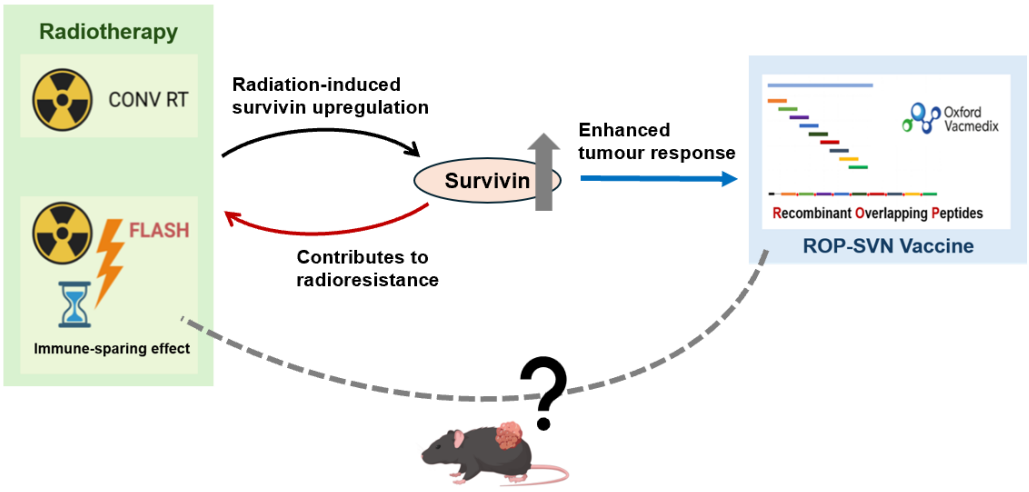


Figure 2. Rationale for combining ROP-SVN vaccination with FLASH radiotherapy. *The rationale for combining ROP-SVN vaccination with FLASH radiotherapy is based on the association between survivin expression and the immune response to ROP-SVN, radiation-induced survivin upregulation, and the normal tissue-sparing effects of FLASH radiotherapy.*

Specifically, we aimed to:

1. Generate a murine survivin-targeting ROP vaccine (ROP-mSVN) to enable evaluation in a physiologically relevant murine model.

2. Investigate the therapeutic efficacy of ROP-mSVN vaccination in combination with FLASH radiotherapy.

2 Method

2.1 Production of ROP-mSVN

2.1.1 cDNA Synthesis

The cDNA sequences encoding ROP-mSVN and its wild-type counterpart (WT-mSVN) were fused with a His-tag and codon-optimised for expression in Escherichia coli (E. coli). The resulting sequences were synthesised and inserted into the pET30 vector backbone by MerryBio.

2.1.2 Bacterial Transformation

Selection agar plates were prepared using LB agar (Sigma, L2897) according to the manufacturer's instructions and supplemented with 50 μg/mL kanamycin (Sigma, K1377). Plasmids were transformed into BL21(DE3) Competent E. coli (New England Biolabs, C2527H) according to the manufacturer’s instructions. Briefly, 50 ng of plasmid DNA was added to 50 μL of competent cells. The cell mixture was incubated on ice for 30 minutes and subjected to heat shock at 42°C for 10 seconds, followed by incubation on ice for 5 minutes. Subsequently, 950 μL of room-temperature SOC Outgrowth Medium was added. The cells were incubated at 37°C for 60 minutes with shaking at 250 rpm. A 50 μL aliquot of the cell culture was then spread onto a selection agar plate and incubated overnight at 37°C.

2.1.3 Colony Screening

A single colony was selected from the selection agar plate and inoculated into 5 mL of LB broth medium (Sigma, L3022) supplemented with 50 μg/mL kanamycin (Sigma, K1377). The culture was incubated overnight at 37°C with shaking at 200 rpm. Following incubation, 500 μL of the cell culture was mixed with 500 μL of sterile 50% glycerol (Thermo Scientific, A16205.AP) in a cryogenic vial (Corning, 430488) and stored at −80°C as glycerol stocks for long-term use. The remaining cell culture was used for small-scale DNA extraction using a miniprep kit (Qiagen, 27104) following the manufacturer's instructions. The extracted DNA was sent to Plasmidsaurus for Sanger sequencing. The resulting sequence data were aligned with the designed sequences using SnapGene to confirm the accuracy of the DNA inserts.

2.1.4 Protein Expression

Selective LB and 2×YT liquid media were prepared using LB (Sigma, L3022) and 2×YT medium (Becton Dickinson, 244020), respectively, according to the manufacturers' instructions and supplemented with 50 μg/mL kanamycin (Sigma, K1377). A pipette tipful of transformed bacterial cells was removed from the glycerol stocks and inoculated into 5 mL of either selective LB or 2×YT medium. Two cultures were prepared for each condition. The cultures were grown overnight at 37°C with shaking at 200 rpm.

The overnight cultures were diluted 1:100 into 1 L of the corresponding selective medium and incubated at 37°C with shaking at 200 rpm until the OD600 reached 0.5. A 1 mL sample was collected as the uninduced control. The remaining culture was used for induction of protein expression. Different induction conditions were evaluated as described in the Results section. The final induction conditions for WT-mSVN and ROP-mSVN were as follows.

i) For WT-mSVN, the culture temperature was reduced to 18°C and IPTG (Thermo Scientific, R0392) was added to a final concentration of 1 mM. The culture was then incubated at 18°C for 24 h with shaking at 200 rpm.

ii) For ROP-mSVN, IPTG (Thermo Scientific, R0392) was added to a final concentration of 1 mM, and the culture was incubated at 37°C for 3 h with shaking at 200 rpm.

Following induction, a 1 mL sample was collected as the induced-cell sample. The remaining culture was harvested by centrifugation for 30 minutes at 5000 × g. The pellet was resuspended in resuspension buffer at a ratio of 10 mL/g. A fresh resuspension buffer was prepared with the following components (**Table 1**).

Table 1. Composition of the resuspension buffer.

Component	Final concentration	Catalogue number
Tris, pH 7.5	50 mM	Trizma Hydrochloride (Sigma, T3253) Trizma Base (Sigma, T1503)
NaCl	0.15 M	Sigma, S5150
TCEP HCI	1 mM	Fluorochem, M02624
Imidazole	10 mM	Sigma, 56750
Igepal CA-630	0.01%	Thermo Scientific, J61055.AE
Glycerol	5%	Thermo Scientific, A16205.AP
Protease inhibitors	1×	Roche, 11873580001

The cell suspension was incubated on ice for 20 minutes. Igepal CA-630 (Thermo Scientific, J61055.AE) was then added to a final concentration of 0.1% and 5 M NaCl (Sigma, S5150) was added to a final concentration of 10%. The cell suspension was sonicated until it was no longer viscous. A 50 µL sample was collected as the crude sample. The remaining lysate was centrifuged for 30 minutes at 5000 × g at 4°C. The supernatant and pellet were collected separately.

The uninduced control, induced-cell, crude, supernatant, and pellet samples were analysed by SDS-PAGE followed by Coomassie Blue staining to assess protein expression and solubility.

2.1.5 Protein Purification

Different purification strategies were used for ROP-mSVN and WT-mSVN according to the solubility of each protein, as described in the Results section.

i) For ROP-mSVN, the pellet was dissolved in 8 M urea (Sigma, 15604) and purified using a gravity column (Cytiva, GE29-0005-94) according to the manufacturer's instructions. The compositions of the binding, wash, and elution buffers are shown in **Table 2.**

Table 2. Composition of the binding, wash and elution buffers for ROP-mSVN.

Component	Catalogue Number	Binding buffer	Wash buffer	Elution buffer
Sodium phosphate	Sodium phosphate monobasic monohydrate (Sigma, S9638) Sodium phosphate dibasic heptahydrate (Sigma, 71640)	50 mM	50 mM	50 mM
NaCl	Sigma, S5150	300 mM	300 mM	300 mM
Imidazole	Sigma, 56750	\	5 mM	150 mM
Urea	Sigma, 15604	8 M	8 M	8 M

For gradient elution, the wash and elution buffers were mixed at different ratios to generate elution solutions containing 25%, 50%, 65%, 75%, and 100% elution buffer.

ii) For WT-mSVN, the supernatant was purified using a gravity column (Cytiva, GE29-0005-94) according to the manufacturer's instructions. The compositions of the binding, wash, and elution buffers are shown in **Table 3**.

Table 3. Composition of the binding, wash and elution buffers for WT-mSVN.

Component	Catalogue Number	Binding buffer	Wash buffer	Elution buffer
Sodium phosphate	Sodium phosphate monobasic monohydrate (Sigma, S9638) Sodium phosphate dibasic heptahydrate (Sigma, 71640)	50 mM	50 mM	50 mM
NaCl	Sigma, S5150	300 mM	300 mM	300 mM
Imidazole	Sigma, 56750	\	5 mM	150 mM
Protease inhibitors	Roche, 11873580001	1×	1×	1×

For gradient elution, the wash and elution buffers were mixed at different ratios to generate elution solutions containing 25%, 50%, 65%, 75%, and 100% elution buffer.

2.1.6 Protein Refolding

The eluted protein samples were refolded by dialysis using Dialysis Tubing (Thermo Scientific, 68700). The compositions of the dialysis buffers used for the first and second dialysis steps are shown in **Table 4**.

Table 4. Composition of the dialysis buffers

Component	Catalogue Number	Dialysis buffer 1	Dialysis buffer 2
PBS	Gibco, 18912	1×	1×
L-Glutathione, reduced	Cayman, 10007461	4 mM	\
L-Glutathione, oxidized	Cambridge bioscience, HY-D0844	0.4 mM	\
L-Arginine	Sigma, W381918	0.4 M	\
Urea	Sigma, 15604	1 M	\
Glycerol	Thermo Scientific, A16205.AP	5%	10%

Each dialysis step was performed for 12–16 h at 4°C. Following dialysis, the protein samples were filtered through a 0.22 μm filter (Millipore, SLGSR33SS), aliquoted, and stored at −80°C.

2.1.7 Protein Electrophoresis

For samples collected during protein expression and purification, 14 μL of sample was mixed with 3 μL of 6× SDS sample buffer (Thermo Scientific, J60660.AC) and 1 μL of 1 M dithiothreitol (DTT, Fluorochem, M02712). For identity confirmation of purified protein, 50 ng of protein was used for electrophoresis with the same SDS and DTT-containing sample buffer. Samples were denatured by heating at 95°C for 10 minutes and loaded onto 14% acrylamide gels together with a protein ladder (Thermo Scientific, 26619). Electrophoresis was performed at 80 V for 20 minutes, followed by 120 V for 60 minutes. Following electrophoresis, the gels were processed by either Coomassie Blue staining or Western blotting, as described in Sections 2.1.8 and 2.1.9, respectively.

2.1.8 Coomassie Protein Staining

The SDS-PAGE gel was incubated with 20 mL of Quick Blue Protein Stain (LubioScience, LU001000) with shaking for 30 minutes at room temperature, followed by washing with distilled water overnight. Protein bands were detected using the imaging System (Bio-Rad).

2.1.9 Western Blot

Proteins were transferred from the SDS-PAGE gel onto a nitrocellulose membrane at 300 mA for 75 minutes on ice. The membrane was then blocked with 5% skimmed milk (VWR,

84615.0500) dissolved in tris-buffered saline with 0.15% Tween (PBST) at room temperature for 1 h. For survivin detection, the membrane was incubated with the primary antibody at 4°C overnight. The membrane was then washed three times with PBST for 10 minutes per wash and incubated with the secondary antibody at room temperature for 60 minutes. For detection of the loading control β-actin, the membrane was incubated with the one-step antibody at room temperature for 60 minutes. Following three washes with PBST, chemiluminescence substrate (Thermo Scientific, 34075) was applied to the membrane. Protein bands were detected using the imaging system (Bio-Rad). A list of antibodies used in this thesis is provided in **Table 6**.

Table 6. Antibodies used for Western blotting.

Antibody	Clone	Catalogue number	Dilution
Anti-survivin	71G4B7	Cell signaling, 2808	1:2000
Anti-rabbit IgG-HRP	N/A	Cell signaling, 7074S	1:5000
Anti-β-actin-HRP	2F1-1	Biolegend, 643807	1:2000

2.1.10 Purity Assay

Protein purity was estimated by comparison with bovine serum albumin (BSA, Sigma, A7030) with a known purity of more than 98%. A total of 5 μg of the purified protein and 5 μg of BSA were loaded onto the same gel, followed by protein electrophoresis and

Coomassie Blue staining as described in Sections 2.1.7 and 2.1.8. The purity of the protein was evaluated using ImageJ. The gel image was converted to 8-bit, and the integrated density (IntDen) of the entire sample lane and the target protein band was measured using rectangular selections. Protein purity was estimated using the following formula.

Target protein purity (%) = [Target protein IntDen / Total lane IntDen] / [BSA band IntDen / Total BSA lane IntDen] × Known BSA purity (%)

2.2 Evaluation of ROP-mSVN combined with FLASH radiotherapy

2.2.1 Licensing

Animal work was conducted in accordance with UK Home Office guidelines and the ARRIVE (Animal Research: Reporting of In Vivo Experiments) guidelines. Mouse experiments were approved by the University of Oxford Animal Welfare and Ethical Review Body (AWERB) under University of Oxford project licences PP8415318 and PP0478598.

2.2.2 Animals

Female C57BL/6J mice were purchased at 5 weeks of age from Charles River UK Ltd. Mice were housed at the Department of Biomedical Services, Radiobiology Research Institute, University of Oxford, Oxford. Mice were housed in individually ventilated cages

under temperature-controlled conditions with a 12-hour reversed light/dark cycle, with lights on at 7:00 AM. Food and water were provided ad libitum.

2.2.3 Cell Culture and Maintenance

B16F10 cells were cultured in DMEM medium (Gibco, 41966029) supplemented with 10% foetal bovine serum (FBS, Sigma, F9665) and 1% penicillin-streptomycin (pen-strep, Gibco, 15140122). When the cells reached approximately 80% confluence, they were washed twice with DPBS (Gibco, 14190094) and dissociated with trypsin-EDTA (Sigma, T3924) at 37°C for 8 minutes. Three volumes of culture medium were added to terminate trypsinisation. The cell suspension was centrifuged at 300 × g for 5 minutes and resuspended in fresh culture medium. Cells were then seeded into a sterile culture flask at a 1:10 split ratio.

For cryopreservation, cells were collected by centrifugation and resuspended in freezing medium containing 90% (v/v) DMEM and 10% (v/v) dimethyl sulfoxide (DMSO, Sigma, D2650). Cell suspensions were transferred into cryogenic vials (Corning, 430488) and stored at −80°C for 24 h before being transferred to liquid nitrogen for long-term storage.

2.2.4 Immunofluorescence

Coverslips were coated with 0.1 mg/mL Poly-D-Lysine (Gibco, A3890401) for 1 h at room temperature and washed twice with DPBS (Gibco, 14190094) to remove excess Poly-D-Lysine before drying in an incubator overnight. Cells were seeded onto the coated coverslips and cultured until approximately 80% confluence. After that, cells were washed with ice-cold DPBS and fixed with ice-cold 2% paraformaldehyde (PFA) for 10 minutes, followed by two washes with DPBS. Next, cells were permeabilised with DPBS containing 0.25% Triton X-100 (Sigma, T9284) for 3 minutes and washed twice with DPBS. Samples were then blocked with DPBS containing 1% BSA (Sigma, A7030) for 1 h at room temperature. Cells were then incubated with an anti-survivin primary antibody (Cell signaling, 2808) diluted 1:100 in DPBS containing 0.1% BSA at room temperature for 1.5 h. Following three washes with DPBS containing 1% BSA, cells were incubated with Coralite anti-rabbit 488 secondary antibody (Proteintech, SA00013-2) at a 1:500 dilution for 1 h. Samples were subsequently washed three times with DPBS and mounted using mountant containing DAPI (Invitrogen, P36941). Images were acquired by an EVOS M5000 microscope (Thermo Scientific, AMF5000SV). Images were processed using ImageJ.

For control staining, B16F10 cells were incubated with a rabbit anti-CD8α primary antibody (Cell Signaling, 85336) under the same conditions as the anti-survivin antibody, followed by the same Coralite anti-rabbit 488 secondary antibody. A secondary antibody-only control was also included, in which the primary antibody incubation step was omitted.

All control samples were processed and imaged using the same procedures described above.

2.2.5 Mycoplasma Test

Cell cultures were tested for mycoplasma contamination using a mycoplasma detection kit (Jena Bioscience, PP-401S). Culture medium was collected immediately before cell splitting and centrifuged at 250 × g for 30 seconds. The supernatant was transferred to a new vial and centrifuged at 15,000 × g for 15 minutes. The pellet was resuspended in 50 µL of Sample Buffer provided with the kit and incubated at 95°C for 5 minutes. A 1 µL aliquot of the prepared sample, Control DNA as the positive control, or Sample Buffer as the negative control was added to 23.5 µL of Master Mix and 0.5 µL of Polymerase. PCR was performed using the programme shown in **Table 7**.

Table 7. PCR programme for mycoplasma detection.

Temperature (°C)	Time (seconds)	Number of cycles
94	120	1
94	30	35
55	30	
72	30	
72	120	1

Following PCR, DNA gel loading buffer was added to each reaction, and the products were analysed by gel electrophoresis. The gel was prepared using agarose (Sigma, 9539) and GelRed (Merck, SCT123). The DNA bands were detected using the imaging System (Bio-Rad). Mycoplasma contamination was indicated by the presence of a band at approximately 270 bp.

2.2.6 Establishment of Tumour Models

B16F10 cells, a murine melanoma cell line with high survivin expression, were selected as the target tumour cell line for evaluation of the ROP-mSVN vaccine. A total of 1×10^5 or 4×10^5 B16F10 cells suspended in PBS were mixed with Matrigel (Corning, 356234) at a final volume of 100 μL at a 1:1 ratio. Seven-week-old C57BL/6 mice were injected subcutaneously with the cell mixture into the right flank. Tumour length and width were measured using a calliper, and tumour volume was calculated according to the following formula.

$$\text{Tumour volume } (mm^3) = [\text{length } (mm) \times \text{width } (mm) \times \text{width } (mm)] / 2$$

Tumour volume was monitored one to three times per week, initially once weekly, with the frequency increased as tumour volume exceeded 500 mm^3. Mice were sacrificed when tumour volume approached the ethical limit of 1200 mm^3.

2.2.7 FLASH Irradiation In Vivo

FLASH irradiation was performed using a 6 MeV electron linear accelerator (LINAC) established at the University of Oxford, as previously described (Berne, Petersson et al. 2021). Mice were anaesthetised with isoflurane at 4% for induction and 2% for maintenance, supplemented with approximately 55% oxygen, generated by evenly mixing 90% oxygen with air. The total duration of anaesthesia was less than 10 minutes. Mice were positioned upright in a mouse cradle in front of the horizontal radiation beam, as previously described (Kersemans, Gilchrist et al. 2021, Ruan, Lee et al. 2021). Irradiation was performed at room temperature using a 6 MeV electron beam. A single dose of 10 Gy was prescribed to the skin surface and delivered at a FLASH dose rate of ≥1800 Gy/s.

2.2.8 Vaccination

ROP-mSVN at a dose of 50 or 100 μg was emulsified with the adjuvant, Montanide (SEPPIC, 36362ZFL2R3) at a final volume of 100 μL at a 1:1 ratio. For the adjuvant control group, 50 μL of PBS was emulsified with 50 μL of Montanide. C57BL/6 mice were injected subcutaneously with the emulsified protein or adjuvant control into the left flank.

To evaluate the immune response induced by ROP-mSVN, tumour-free mice received three immunisations, consisting of one initial immunisation followed by two booster

injections administered at 7-day intervals. Mice receiving PBS emulsified with Montanide were used as controls.

To evaluate the therapeutic efficacy of FLASH radiotherapy in combination with ROP-mSVN vaccination, tumour-bearing mice with or without FLASH radiotherapy treatment were immunised with ROP-mSVN on days 5, 15, and 20 after tumour inoculation.

2.2.9 Serum Collection

Approximately 100 μL of blood was collected from the tail vein of each C57BL/6 mouse. An incision was made perpendicular to the tail vein at approximately two-thirds of the distance from the base of the tail, and blood was collected into an Eppendorf tube without anticoagulant. Blood samples were allowed to stand for 30 minutes at room temperature and then centrifuged at 1000 × g for 15 minutes. The supernatant was collected as serum, aliquoted, and stored at −80°C.

2.2.10 ELISA

96-well plates were coated with 100 μL of WT-SVN protein diluted to 2 μg/mL in PBS and incubated overnight at 4°C. The plates were then washed three times with PBS

containing 0.05% Tween-20 (PBST). Each well was blocked with 100 µL of 5% BSA (Sigma, A7030) in PBS at 37°C for 2 h.

Serum samples were diluted in PBS at 1:1000, 1:10,000, and 1:100,000, with a final volume of 100 µL, and added to wells in duplicate. The plates were incubated at 37°C for 1 h. The serum samples were then removed, and the wells were washed three times with PBS. HRP-conjugated anti-mouse IgG antibody (Abcam, ab205719) diluted in PBS to a final concentration of 0.2 µg/mL was added and incubated at 37°C for 45 minutes. Following three washes with PBST, 100 µL of 3,3′,5,5′-tetramethylbenzidine (TMB) solution (Biolegend, 421501) was added to each well. After approximately 5 minutes, 100 µL of ELISA stop solution (Cambridge bioscience, E115) was added. Absorbance was measured at 450 nm using a microplate reader (Thermo Scientific). Antibody titres were defined as the highest serum dilution that produced an OD450 value above 0.2, which was used as the threshold for detectable anti-SVN antibody responses (Fuller, Takahashi et al. 1992).

2.2.11 Isolation of Splenocytes

Spleens were harvested from C57BL/6J mice immediately after euthanasia. Each spleen was mechanically dissociated through a 100 µm cell strainer (Falcon, 352360) using RPMI 1640 (Gibco, 21875) to generate a single-cell suspension. The suspension was further

purified by Ficoll density-gradient centrifugation using Ficoll-Paque media (Cytiva, GE17-5446-02) according to the manufacturer's instructions. Briefly, 3 mL of Ficoll-Paque media was added to a 15 mL centrifuge tube, and 4 mL of the cell suspension was carefully layered onto the Ficoll-Paque solution. The samples were centrifuged at 400 × g for 30 minutes at room temperature with acceleration set to 1 and deceleration set to 0. The mononuclear cell layer was transferred to a fresh centrifuge tube and washed with RPMI 1640. The isolated splenocytes were cultured in RPMI 1640 supplemented with 10% foetal bovine serum (FBS, Sigma, F9665) and 1% penicillin-streptomycin (pen-strep, Gibco, 15140122) and used for ELISpot analysis within 6 h of tissue collection.

2.2.12 ELISpot

Hydrophobic PVDF 96-well plates (Millipore, M8IPS4510) were treated with 20 µL of 35% ethanol for 30 seconds to facilitate binding of the capture antibody. The plates were washed five times with sterile water and coated with 100 µL of anti-IFN-γ antibody (Mabtech, 3321-3A) at a concentration of 15 µg/mL overnight at 4°C. Following five washes with DPBS (Gibco, 14190094), 200 µL of RPMI 1640 was added to each well and incubated for 1 h at room temperature to block non-specific binding.

ROP-SVN was used as the stimulus, while Concanavalin A (ConA, Sigma, C0412) and RPMI 1640 (Gibco, 21875) were used as positive and negative controls, respectively. A

50 µL aliquot of ROP-SVN (5 µg/mL), ConA (2 µg/mL), or RPMI 1640 was mixed with 50 µL of splenocyte suspension containing 2.5×10^6 cells and added to the corresponding wells. The plate was covered with aluminium foil and incubated at 37°C in a humidified incubator with 5% CO_2 for 18 h.

Following five washes with DPBS, 100 µL of biotinylated anti-IFN-γ antibody (Mabtech, 3321-3A) diluted to 1 µg/mL in DPBS containing 0.5% foetal bovine serum (FBS, Sigma, F9665) was added to each well and incubated at 37°C for 2 h. The plate was then incubated with 100 µL of Streptavidin-ALP (Mabtech, 3321-3A) diluted at 1:1000 in DPBS containing 0.5% FBS. 100 µL of BCIP/NBT-plus substrate (Mabtech, 3650-10) was subsequently added to develop the spots. Once distinct spots had developed, typically within 5–30 minutes, colour development was stopped by thorough washing with tap water. The plate was allowed to dry overnight before analysis.

2.3 Data Analysis

Statistical analyses were performed using GraphPad Prism 10, and image analysis was performed using ImageJ.

3 Results

3.1 Production of ROP-mSVN

3.1.1 Recombinant ROP-mSVN protein expression

ROP-mSVN construct design

The design of the ROP-mSVN sequence is illustrated in **Figure 3**. The wild-type survivin sequence was divided into eight overlapping fragments, connected by a four-amino-acid linker sequence, Leu-Arg-Met-Lys (LRMK). The design rationale and strategy are detailed in Section 1.3.1 above. An N-terminal His-tag was incorporated into the ROP-mSVN sequence to facilitate subsequent purification of the recombinant protein.

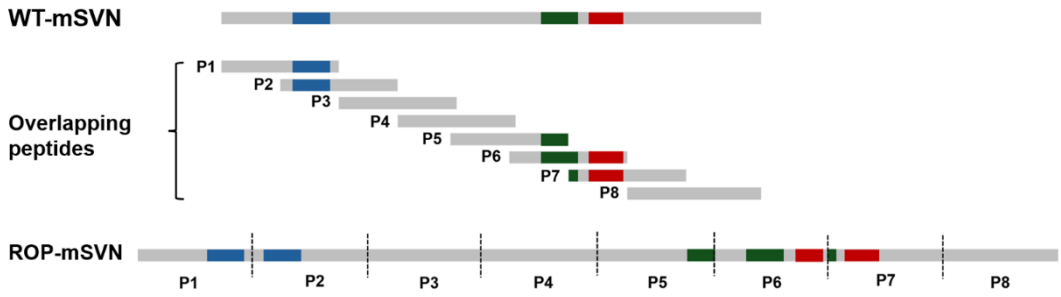


Figure 3. Graphical representation of the ROP-mSVN vaccine construct. *The wild-type mouse survivin sequence (WT-mSVN) was divided into eight overlapping peptide fragments, each comprising around 30 amino acids with a 15-amino-acid overlap between adjacent fragments. The fragments were linked by Leu-Arg-Met-Lys (LRMK) linker sequences to generate the ROP-mSVN construct. Different colours represent T-cell epitopes within the WT-mSVN sequence identified from the Immune Epitope Database*

(IEDB). P1–P8, overlapping mouse survivin peptide fragments; dashed vertical lines, LRMK linker sequences.

E. coli was selected as the expression system for ROP-mSVN production because of its established suitability for the high-level production of recombinant proteins and the intended use of ROP-mSVN as a vaccine antigen (Schütz, Bernhard et al. 2023). Accordingly, the ROP-mSVN coding sequence was codon-optimised for E. coli expression before being inserted into the pET-30 expression vector.

Investigation of conditions for ROP-mSVN expression

Following construction of the ROP-mSVN plasmid, it was transformed into BL21(DE3) competent cells. Protein expression was induced using isopropyl β-D-1-thiogalactopyranoside (IPTG), a will-established inducer of recombinant protein expression (Munro, Ackers et al. 2016). An initial IPTG concentration of 1 mM was selected based on commonly used conditions for protein expression (Kormanová, Rybecká et al. 2020). 2×YT medium, a nutrient-rich medium that provides favourable conditions for bacterial growth (Rosano and Ceccarelli 2014), was initially used for bacterial culture. To explore suitable conditions for ROP-mSVN expression, two induction conditions were initially tested in small-scale cultures, where IPTG induction was performed at either 18°C for 24 h or 37°C for 3 h. After induction, the bacterial cells were resuspended in a detergent-containing buffer, followed by sonication for cell lysis. The lysates were

subsequently centrifuged to separate the soluble and insoluble fractions, which were analysed by SDS-PAGE with Coomassie staining (**Figure 4**). Compared with the uninduced control, a distinct band with enhanced intensity was observed in the pellet fraction under both induction conditions, with the corresponding band barely detectable in the supernatant fractions. The molecular weight of this band was consistent with the predicted molecular weight of ROP-mSVN (33 kDa), as calculated using the ExPASy tool. These results suggested that ROP-mSVN was expressed primarily in an insoluble form. Notably, the band at 37°C was more clearly defined than the one at 18°C.

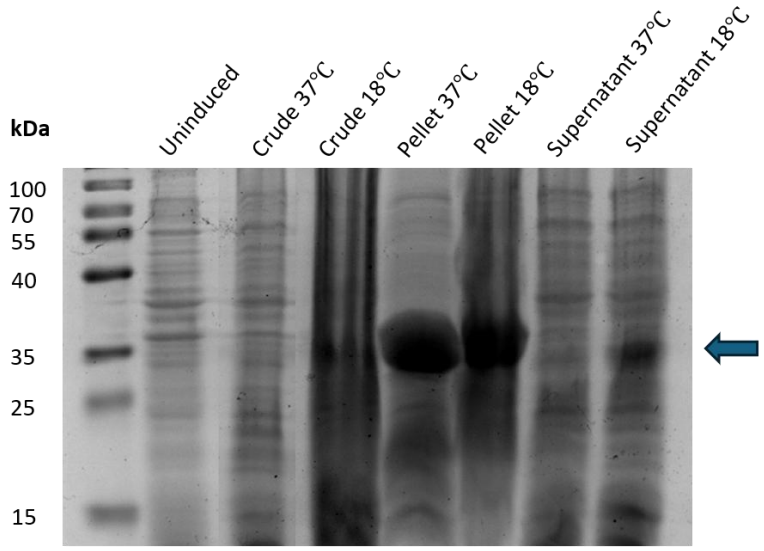


Figure 4. Expression of ROP-mSVN under different induction conditions. *ROP-mSVN expression was assessed by SDS-PAGE following induction with 1 mM IPTG at either 37°C for 3 h or 18°C for 24 h. The protein ladder is indicated. ROP-mSVN was detected at the predicted molecular weight of approximately 33 kDa under both induction conditions, with most of the protein present in the pellet. Crude, resuspended bacterial cells collected after induction and before sonication; supernatant, soluble fraction collected after*

sonication and centrifugation; pellet, insoluble fraction collected after sonication and centrifugation; blue arrow, predicted molecular weight of ROP-mSVN (33 kDa).

As purification from insoluble fractions generally requires additional processing steps, further investigation was conducted to determine whether the solubility of ROP-mSVN could be improved. Lower induction temperatures and reduced IPTG concentrations have previously been reported as strategies for improving the solubility of recombinant proteins (Francis and Page 2010). Therefore, a lower IPTG concentration of 0.5 mM was tested at 18°C for 24 h. However, no band corresponding to the predicted molecular weight of ROP-mSVN was observed under this condition (**Figure 5**), suggesting that protein expression was not successfully induced. Accordingly, 1 mM was retained as the IPTG concentration for subsequent experiments. The 37°C induction condition was selected as the band was more clearly defined than that observed at 18°C in the initial experiment (**Figure 4**).

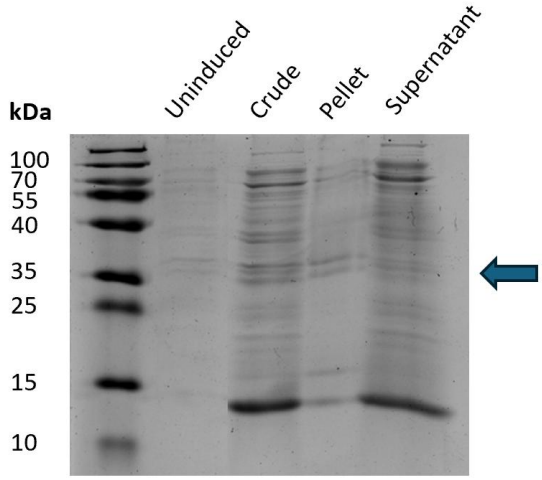


Figure 5. Expression of ROP-mSVN under reduced IPTG concentration. *ROP-mSVN expression was assessed by SDS-PAGE following induction with 0.5 mM IPTG at 18°C for*

24 h. The protein ladder is indicated. No distinct band corresponding to the predicted molecular weight of ROP-mSVN (33 kDa) was observed under this induction condition. Crude, resuspended bacterial cells collected after induction and before sonication; supernatant, soluble fraction collected after sonication and centrifugation; pellet, insoluble fraction collected after sonication and centrifugation; blue arrow, predicted molecular weight of ROP-mSVN (33 kDa).

Given the greater availability of LB medium compared with 2×YT medium, LB medium was subsequently tested for ROP-mSVN expression. Under the induction conditions established above (1 mM IPTG, 37°C for 3 h), ROP-mSVN expression was evaluated following bacterial culture in LB medium. A distinct band at the predicted molecular weight of ROP-mSVN was observed with enhanced intensity in the induced sample (**Figure 6**), indicating that LB medium was also suitable for ROP-mSVN expression.

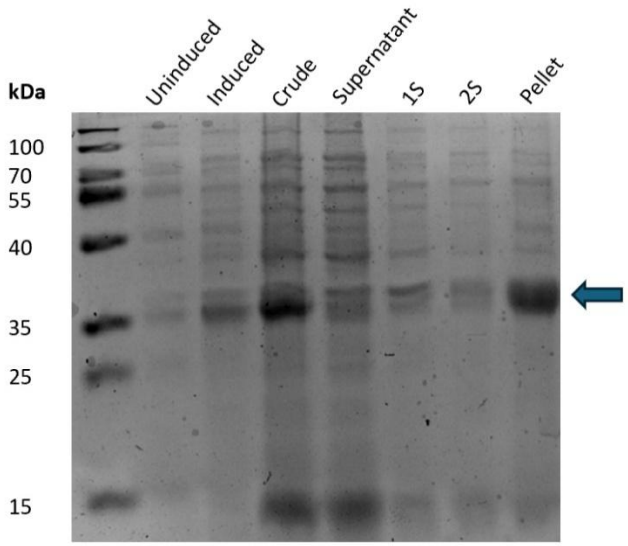


Figure 6. Expression of ROP-mSVN in LB medium. *ROP-mSVN expression was assessed by SDS-PAGE following induction with 1 mM IPTG at 37°C for 3 h in LB medium. The protein ladder is indicated. A prominent band corresponding to the predicted molecular weight of ROP-mSVN was observed in the insoluble fraction, while only weak bands were observed in the 1S and 2S fractions. Crude, resuspended bacterial cells collected after induction and before sonication; supernatant, soluble fraction collected after sonication and centrifugation; pellet, insoluble fraction collected after sonication and centrifugation; 1S and 2S, supernatants collected following washing of the insoluble fraction with 1 M and 2 M urea, respectively; blue arrow, predicted molecular weight of ROP-mSVN (33 kDa).*

Based on the findings above, large-scale ROP-mSVN expression was subsequently performed under the established conditions (1 mM IPTG, 3 h, 37°C, LB medium). Wild-type mouse survivin (WT-mSVN) cloned into the same expression vector was induced in parallel as a comparison. Consistent with the findings from the small-scale experiments,

ROP-mSVN was mainly detected in the insoluble fraction. Notably, WT-mSVN showed stronger expression in the soluble fraction (**Figure 7**), indicating that the induced WT-mSVN was largely soluble.

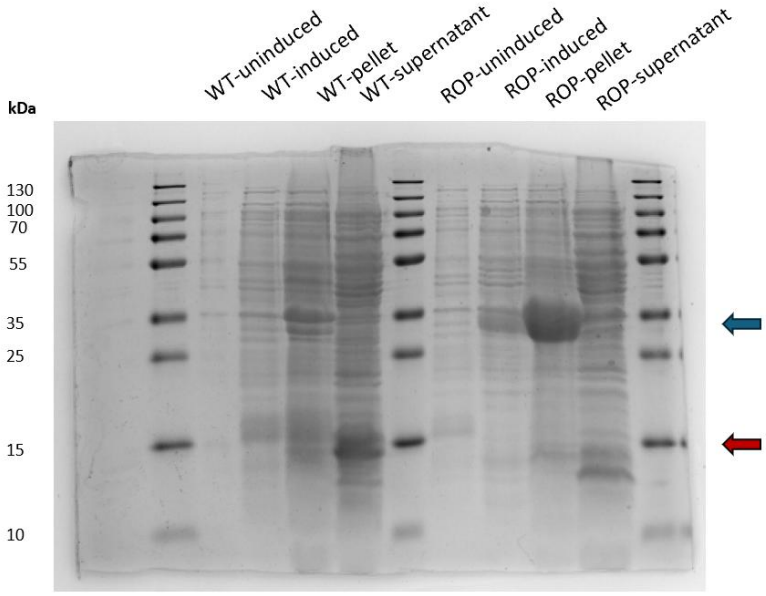


Figure 7. Expression of WT-mSVN and ROP-mSVN. *WT-mSVN and ROP-mSVN expression was assessed by SDS-PAGE. The protein ladder is indicated. WT-mSVN was mainly detected in the supernatant, while ROP-mSVN was mainly detected in the pellet. Red arrow, molecular weight of WT-mSVN (17 kDa); blue arrow, predicted molecular weight of ROP-mSVN (33 kDa). WT, WT-mSVN; ROP, ROP-mSVN; supernatant, soluble fraction collected after sonication and centrifugation; pellet, insoluble fraction collected after sonication and centrifugation.*

Taken together, ROP-mSVN expression was successfully induced. In contrast to the largely soluble WT-mSVN, ROP-mSVN was mainly present in the insoluble fraction,

suggesting that subsequent purification of ROP-mSVN would require a purification strategy for insoluble proteins.

3.1.2 Recombinant ROP-mSVN protein purification

As shown in Section 3.1.1, ROP-mSVN was mainly expressed in the insoluble fraction following IPTG induction. The protein was subsequently purified from the insoluble fraction by immobilised metal affinity chromatography (IMAC), based on the interaction between the His-tag incorporated into ROP-mSVN and immobilised metal ions.

IMAC purification

A cobalt-based affinity resin was selected instead of the more commonly used nickel resin as cobalt generally provides higher selectivity for His-tagged proteins and can therefore reduce non-specific binding of host proteins (Chen, Nomani et al. 2017). Unlike soluble WT-SVN, which could be directly loaded onto the affinity column under non-denaturing conditions, ROP-mSVN required solubilisation under denaturing conditions. The protein was therefore dissolved in buffer containing 8 M urea before loading onto the column. The overall purification procedure is shown in **Figure 8**.

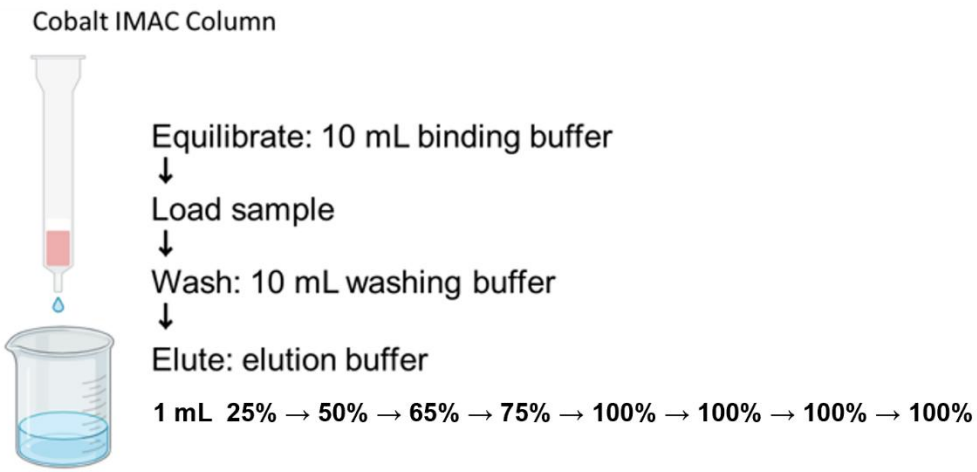


Figure 8. Workflow for ROP-mSVN purification by cobalt immobilised metal affinity chromatography (IMAC). *The cobalt IMAC column was equilibrated with 10 mL binding buffer before sample loading, followed by washing with 10 mL washing buffer. ROP-mSVN was eluted in 1 mL fractions using stepwise gradients of 25%, 50%, 65%, 75% and 100% elution buffer. For the 25%, 50%, 65% and 75% gradients, the remaining proportion was made up of washing buffer. Four consecutive 1 mL fractions were collected using 100% elution buffer.*

To minimise non-specific binding and facilitate separation of ROP-mSVN from other bacterial proteins, the bound proteins were eluted using increasing concentrations of imidazole. The elution fractions are shown in **Figure 9**. Fractions E3–E5, corresponding to 65%, 75% and 100% of the 150 mM imidazole elution buffer, respectively, contained high-intensity bands at the expected molecular weight of ROP-mSVN with relatively limited additional protein bands. These fractions were therefore collected and subjected to subsequent dialysis. Notably, a substantial amount of protein at the expected molecular

weight was also detected in the flow-through fraction, suggesting that the amount of protein loaded may have exceeded the binding capacity of the column. A lower protein loading amount per column would therefore be appropriate for subsequent purification.

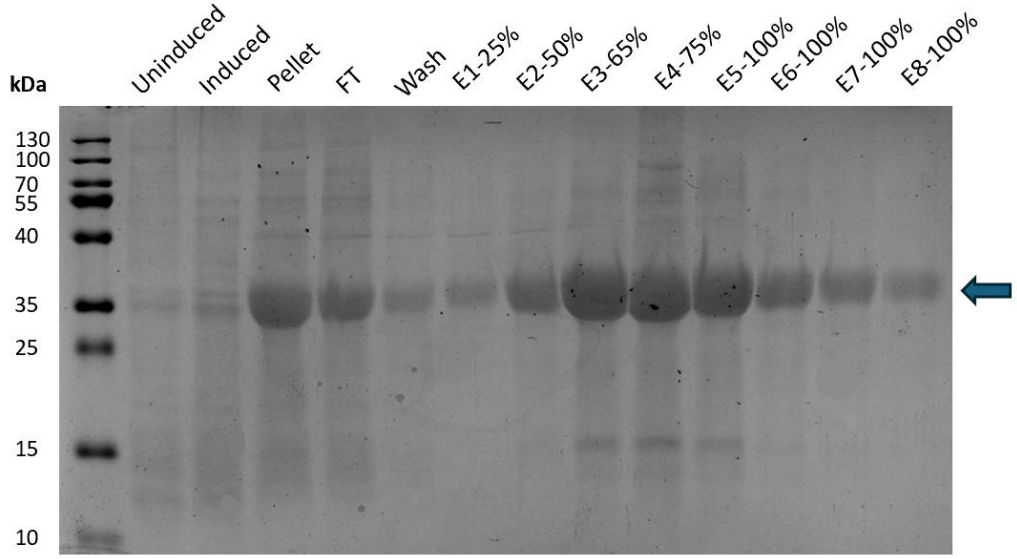


Figure 9. ROP-mSVN purification by cobalt IMAC. *ROP-mSVN purification fractions were analysed by SDS-PAGE. The protein ladder is indicated. The strongest bands corresponding to ROP-mSVN were observed in fractions E3–E5. Pellet, insoluble fraction collected after sonication and centrifugation; FT, flow-through fraction collected after sample loading; Wash, fraction collected during the washing step; E1–E8, elution fractions collected using stepwise elution gradients.*

WT-SVN was purified using a similar affinity chromatography procedure, except that urea was not included as the WT-SVN remained soluble under the purification conditions. Protease inhibitors were additionally included to minimise potential degradation of the

non-denatured protein during purification. The resulting purification profile is shown in **Figure 10**.

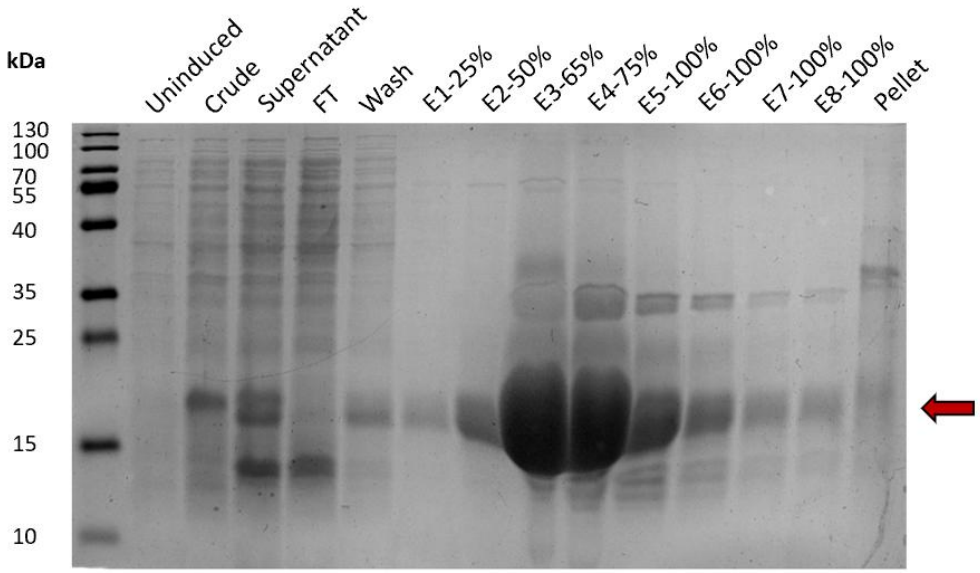


Figure 10. WT-mSVN purification by cobalt IMAC. *WT-mSVN purification fractions were analysed by SDS-PAGE. The protein ladder is indicated. The strongest bands corresponding to WT-mSVN were observed in fractions E3–E4. Crude, resuspended bacterial cells collected after induction and before sonication; Supernatant, soluble fraction collected after sonication and centrifugation; FT, flow-through fraction collected after sample loading; Wash, fraction collected during the washing step; E1–E8, elution fractions collected using stepwise elution gradients; Pellet, insoluble fraction collected after sonication and centrifugation.*

Dialysis

Following affinity purification, the collected ROP-mSVN fractions were subjected to dialysis to remove urea and other low-molecular-weight components from the elution buffer. As direct removal of the denaturant may promote protein aggregation during refolding, a two-step dilution procedure was employed to gradually reduce the urea concentration prior to dialysis, as illustrated in **Figure 11**.

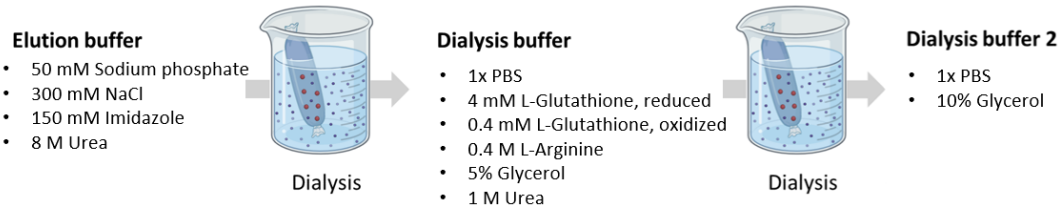


Figure 11. Dialysis procedure for ROP-mSVN refolding. *The purified protein sample was sequentially dialysed against buffers containing decreasing concentrations of urea. The final dialysis was performed against dialysis buffer 2, composed of 1× PBS and 10% glycerol.*

The protein profiles following dialysis are shown in **Figure 12**. A distinct band at approximately 33 kDa was observed in the ROP-mSVN lane, consistent with the predicted molecular weight of ROP-mSVN, although its identity required further confirmation by Western blotting. Notably, the corresponding WT-SVN sample displayed two closely spaced bands of similar molecular weight. The identities of the purified proteins and the nature of the two WT-mSVN bands were subsequently investigated in the next section.

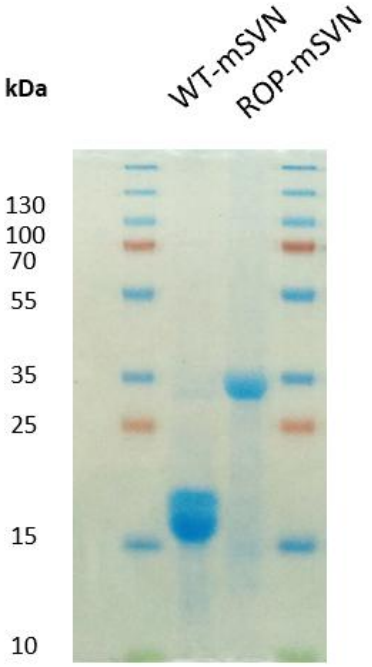


Figure 12. Dialysed WT-mSVN and ROP-mSVN. *Dialysed WT-mSVN and ROP-mSVN were analysed by SDS-PAGE with Coomassie Brilliant Blue staining. The protein ladder is indicated. WT-mSVN and ROP-mSVN were detected at their predicted molecular weights of approximately 17 kDa and 33 kDa, respectively.*

3.1.3 Identity confirmation

Following dialysis, the purified ROP-mSVN protein showed a band at a molecular weight consistent with its predicted size on SDS-PAGE. Its identity was subsequently verified by Western blotting using a commercially available antibody against wild-type survivin. As shown in **Figure 13**, a prominent immunoreactive band was detected at the expected molecular weight of ROP-mSVN, supporting the identity of the purified recombinant

protein as ROP-mSVN. This also indicated that the recombinant protein retained an epitope recognised by the anti-survivin antibody.

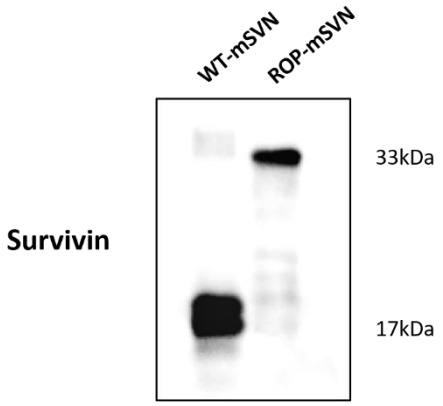


Figure 13. Western blot detection of purified WT-mSVN and ROP-mSVN. *Purified WT-mSVN and ROP-mSVN were analysed by Western blotting using the same anti-survivin antibody. Bands were detected at approximately 17 kDa and 33 kDa, corresponding to the expected molecular weights of WT-mSVN and ROP-mSVN, respectively.*

Consistent with the Coomassie-stained gel, two closely spaced immunoreactive bands were observed at the molecular weight range expected for WT-SVN (**Figure 12, Figure 13**). Similar double bands have previously been reported for survivin and attributed to alternatively spliced survivin isoforms (Conway, Pollefeyt et al. 2000, Jarrin, Mansergh et al. 2012). However, the recombinant protein was expressed in E. coli, a prokaryotic system that lacks the canonical pre-mRNA splicing machinery found in eukaryotic cells (Zhiguo, Wang et al. 2013). Therefore, alternative splicing is unlikely to account for the two bands observed here.

To investigate whether the additional band could instead result from protein degradation, an exploratory experiment was performed. Samples were incubated at 4°C for different durations and compared with samples stored at −80°C. For each time point, samples were either boiled at 95°C before electrophoresis or analysed without boiling. Incubation at 4°C was used to allow potential protein degradation, while boiling was used to fully denature the protein before electrophoresis. As shown in **Figure 14**, the relative intensities of the two WT-SVN bands remained comparable across the different incubation and treatment conditions. No progressive loss of either band was observed following incubation at 4°C. These findings did not support protein degradation as the primary explanation for the two-band pattern. The origin of the two bands therefore remains unclear. A less well-established modification of mouse survivin in an E. coli expression system may be a possible explanation, although further investigation is required.

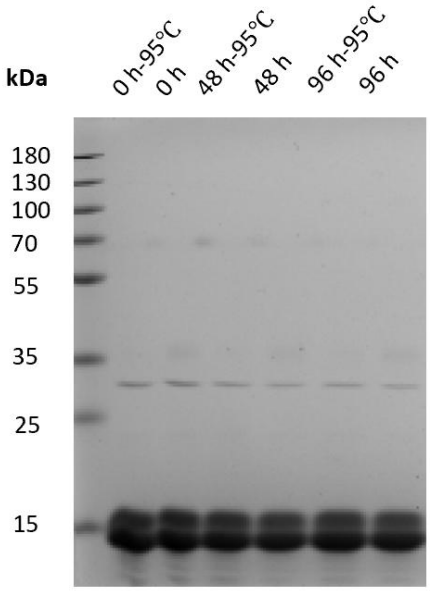


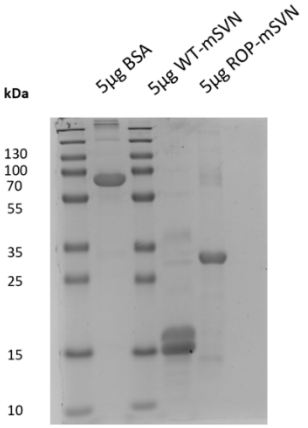
Figure 14. Analysis of the double-band pattern of WT-mSVN. *WT-mSVN samples were incubated at 4°C for 48 or 96 h, with samples analysed either after heating at 95°C or without heating. A sample stored at −80°C and heated at 95°C was included as the 0 h reference. The protein ladder is indicated. The relative intensities of the two WT-mSVN bands remained comparable across the different incubation and treatment conditions, with no progressive loss of either band following incubation at 4°C.*

3.1.4 Purity assessment

Following confirmation of protein identity, the purity of the recombinant ROP-mSVN sample was assessed by comparison with a commercially available high-purity bovine serum albumin (BSA) standard. Equal amounts of the recombinant protein samples and BSA were resolved on the same SDS-PAGE gel and visualised by Coomassie Brilliant

Blue staining, as shown in **Figure 15A**. The intensity of the protein bands was quantified using ImageJ, and the relative purity of recombinant protein was estimated by comparison with the BSA standard (**Figure 15B**).

A)



B)

Sample	Band IntDen	Total lane IntDen	Band/Total	Reference BSA purity (%)	Estimated purity (%)
BSA standard	4.32	45.16	0.09566	98	—
ROP-mSVN	3.962	48.69	0.08817	—	90.3
WT-mSVN	4.54	48.69	0.09332	—	95.6

Figure 15. Estimation of WT-mSVN and ROP-mSVN purity using BSA as a reference. *A) Coomassie-stained SDS-PAGE gel loaded with 5 µg BSA, WT-mSVN and ROP-mSVN. The protein ladder is indicated. B) Band intensity measurements and purity estimation. Band IntDen, integrated density of the target protein band; Total lane IntDen, integrated density of the corresponding lane; Band/total, ratio of band IntDen to total lane IntDen; Reference BSA purity, known purity of the BSA standard; Estimated purity, calculated purity of WT-mSVN or ROP-mSVN based on the BSA reference.*

The estimated purity of ROP-mSVN was approximately 90%, with WT-mSVN showing a higher estimated purity. These results indicated that the purification procedure produced

recombinant proteins with a relatively high degree of purity, supporting the use of the purified ROP-mSVN as a protein antigen in the subsequent mouse vaccination study.

3.2 Evaluation of ROP-mSVN combined with FLASH radiotherapy

3.2.1 Immunogenicity evaluation of the ROP-mSVN vaccine

Experimental design

Following confirmation of the identity and purity of recombinant ROP-mSVN, its functional activity as a vaccine antigen was evaluated in tumour-free C57BL/6 mice. The subcutaneous route was selected for administration of ROP-mSVN in mice, given that it is commonly used for vaccine delivery in clinical studies (Wang, Ji et al. 2024), including for the ROP-hSVN vaccine (Wijaya, Morris et al. 2026). Compared with intravenous administration, subcutaneous administration offers greater patient comfort and improved treatment compliance (Fathallah, Bankert et al. 2013). Following subcutaneous administration, protein antigens can reach lymph nodes through lymphatic transport and be processed by lymph node-resident antigen-presenting cells, or be captured by cutaneous dendritic cells that migrate to the draining lymph nodes (Fathallah, Bankert et al. 2013).

As illustrated in **Figure 16**, mice received three subcutaneous immunisations with ROP-mSVN in the left flank at weekly intervals. Two vaccine doses, 50 μg and 100 μg per injection, were evaluated based on doses used in previous ROP-hSVN studies, with the

adjuvant-only group serving as the control (Cai, Zhang et al. 2017, Zhang, Zhou et al. 2023). Three mice were included in each group in accordance with the Reduction principle of the 3Rs (Verderio, Lecchi et al. 2023). Serum samples were collected four days after the third immunisation for assessment of antibody responses, while spleens were collected seven days after the final immunisation for evaluation of antigen-specific T-cell responses.

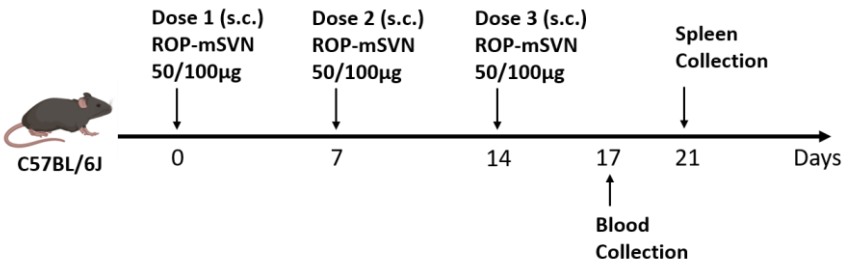


Figure 16. Immunisation schedule for ROP-mSVN vaccination in C57BL/6J mice. *C57BL/6J mice (n=3 per group) received three subcutaneous (s.c.) doses of ROP-mSVN at 50 or 100 µg, or adjuvant as a control, on days 0, 7 and 14. Blood was collected on day 17, followed by spleen collection on day 21.*

Humoral immune response

Serum antibody responses were assessed by ELISA following the third immunisation. As shown in **Figure 17**, anti-survivin antibodies were detected in sera from mice immunised with ROP-mSVN. All vaccinated mice exhibited antibody titres of at least 1:1,000, while no detectable antibody responses were observed in the adjuvant controls. Notably, the 100 µg vaccine group reached a higher maximum antibody titre than the 50 µg group, with the highest titre reaching 1:100,000 compared with 1:10,000 in the 50 µg group. However, this

finding should be interpreted with caution, as variability within groups and the small sample size (n=3) limited the robustness of comparisons between the two doses.

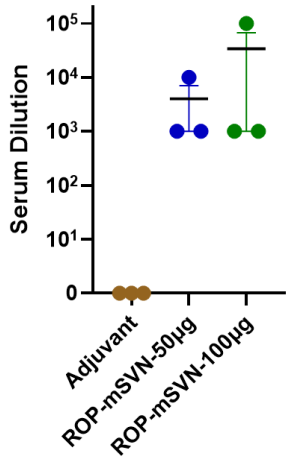


Figure 17. Anti-SVN antibody titres following ROP-mSVN vaccination. *Anti-SVN antibody titres were determined by ELISA. Titres were defined as the highest serum dilution yielding an optical density (OD) > 0.2 at 450 nm. No detectable anti-SVN antibody titre was observed in the adjuvant control group, while both the 50 and 100 µg ROP-mSVN groups showed antibody titres of at least 1,000. Data are presented as mean ± SEM.*

Cellular immune response

Antigen-specific T-cell responses were subsequently assessed using an ELISpot assay. Splenocytes were collected seven days after the third immunisation and stimulated with ROP-mSVN. Concanavalin A (ConA) was used as non-specific positive control, while RPMI 1640 medium alone served as the negative control.

As shown in **Figure 18**, abundant spot formation was observed in the ConA-stimulated positive-control wells from both adjuvant-only and ROP-mSVN-immunised mice, while

minimal spot formation was observed in the negative-control wells, confirming the validity of the assay. ROP-mSVN stimulation resulted in a moderate number of spots in splenocytes from ROP-mSVN-immunised mice, while few or no spots were observed in the adjuvant control group, indicating that ROP-mSVN vaccination induced an antigen-specific cellular immune response.

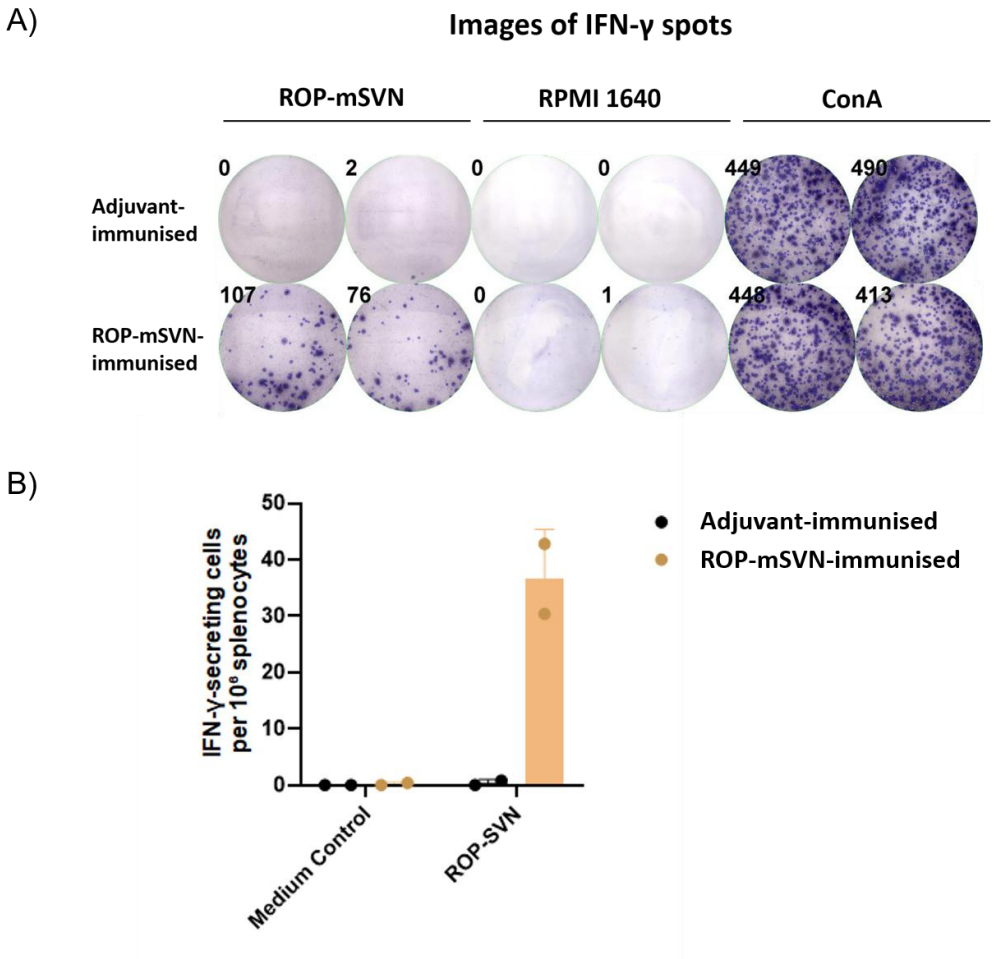


Figure 18. ELISPOT responses of splenocytes following ROP-mSVN vaccination. *A) Representative ELISPOT images of splenocytes from adjuvant-immunised and ROP-mSVN-immunised mice stimulated with ROP-mSVN, RPMI 1640 or concanavalin A (ConA). B) Quantification of IFN-γ spot-forming cells following stimulation with Medium control or ROP-mSVN. Data are presented as mean ± SD of two technical replicates.*

Vaccine tolerability

Mouse body weight was monitored throughout the immunisation period as an indicator of general tolerability. As shown in **Figure 19**, no mouse exhibited a body weight reduction exceeding 10% during the immunisation period. No other vaccine-associated health concerns, including apparent changes in behaviour or general appearance, were observed or reported during the experimental period, suggesting that ROP-mSVN was well tolerated and suitable for subsequent evaluation in tumour-bearing mice.

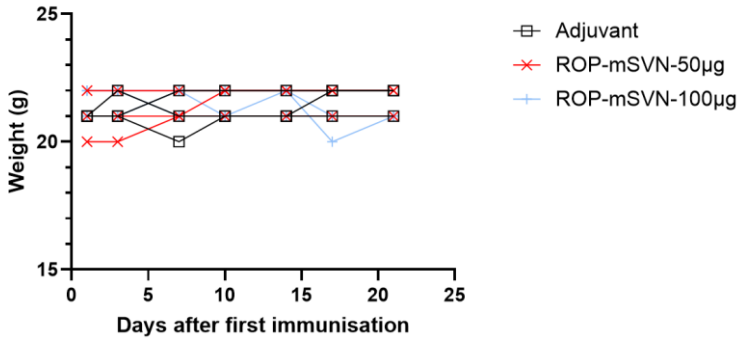


Figure 19. Body weight of mice during the immunisation period. *Body weight was monitored on days 1, 3, 7, 10, 14, 17 and 21 following the first immunisation. Individual mice are shown as separate trajectories for the adjuvant control, ROP-mSVN-50 µg and ROP-mSVN-100 µg groups (n = 3 per group). No mouse exhibited a body weight reduction exceeding 10% during the immunisation period.*

3.2.2 Establishment of the B16F10 melanoma model

Following the successful production of the ROP-mSVN vaccine, a syngeneic B16F10 melanoma model was established for subsequent therapeutic experiments. As a melanoma cell line derived from C57BL/6 mice, B16F10 is able to form tumours in syngeneic immunocompetent mice, allowing antitumour immune responses to be evaluated in an intact immune system (Fowlkes, Clemons et al. 2019). Despite its relatively low immunogenicity, B16F10 has been widely used to evaluate therapeutic cancer vaccines (Kochenderfer, Gress et al. 2007, Zahedipour, Zamani et al. 2023). More specifically, B16F10 was used in preliminary studies of the ROP-hSVN vaccine (Zhang, Zhou et al. 2023) and has also been employed to investigate FLASH radiotherapy in combination with other immunotherapeutic approaches (Dong, Nieves et al. 2023).

Survivin expression in B16F10 cells

Survivin protein expression in B16F10 cells was first examined by Western blotting. As shown in **Figure 20A**, a clear survivin band was detected in B16F10 cell lysates, confirming expression of the target antigen in B16F10 cells. The cellular distribution of survivin was further examined by immunofluorescence staining. As shown in **Figure 20B**, fluorescence corresponding to survivin was detected in both the nucleus and cytoplasm. Collectively, these findings confirmed survivin expression in B16F10 cells, supporting their suitability for subsequent evaluation of ROP-mSVN-induced anti-tumour responses.

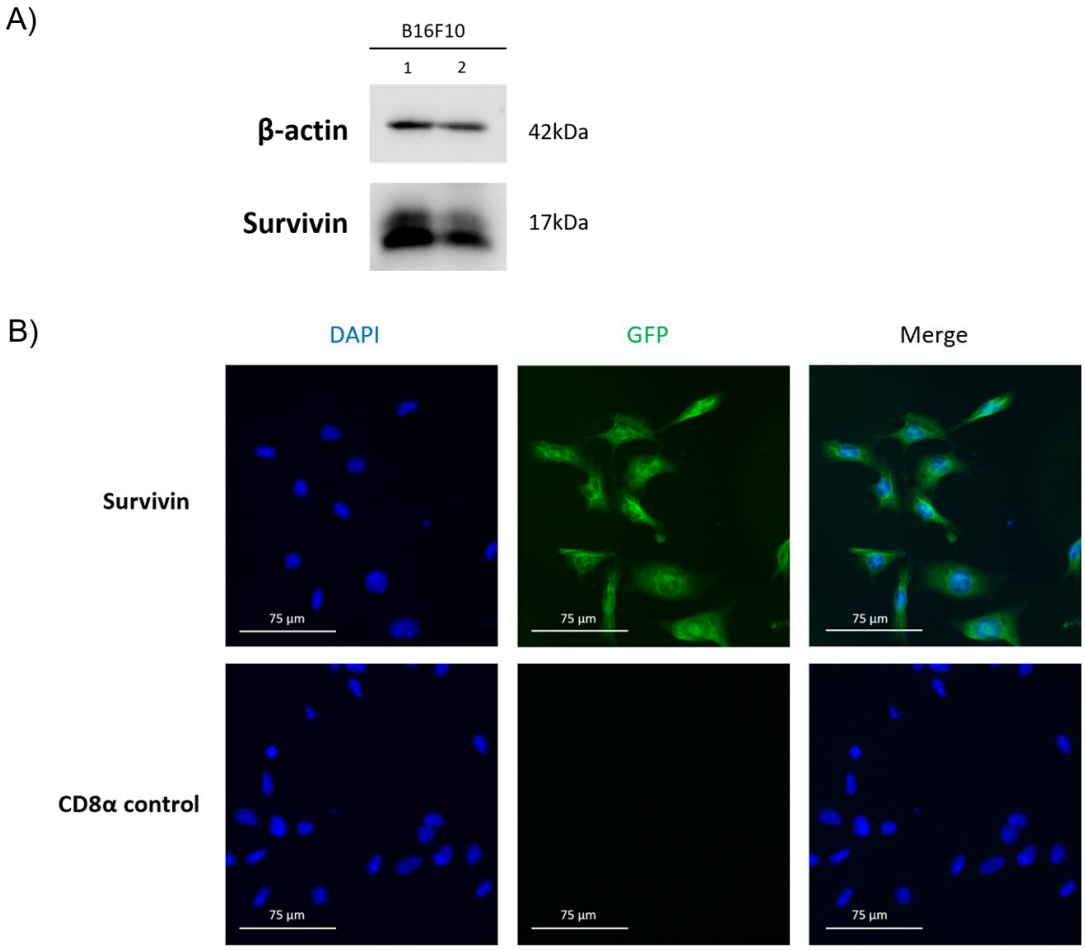


Figure 20. Survivin expression and localisation in B16F10 cells. *A) Western blot analysis of survivin expression in two B16F10 cell samples from independent cryovials (lanes 1 and 2). β-actin was used as a loading control. B) Immunofluorescence staining of survivin in B16F10 cells. Survivin was detected using a rabbit anti-survivin primary antibody followed by a Coralite 488-conjugated secondary antibody. A rabbit anti-CD8α antibody with the same secondary antibody was included as a negative control. DAPI was used for nuclear staining, and merged images show the localisation of survivin relative to the nuclei. Scale bars show 75 µm.*

Mycoplasma testing

As mycoplasma contamination can alter cellular physiology and potentially affect tumour growth in vivo, B16F10 cells were tested for mycoplasma contamination before use in animals. A commercial mycoplasma detection kit was used, and the resulting PCR products were analysed by gel electrophoresis. As shown in **Figure 21**, a band at approximately 270 bp was detected in the positive control but not in the negative control, confirming appropriate assay performance. No corresponding band was detected in the B16F10 cell sample, indicating that the sample was negative for detectable mycoplasma contamination.

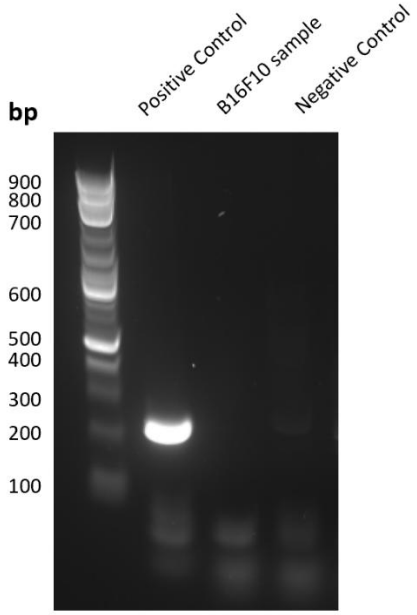


Figure 21. Mycoplasma testing of B16F10 cells. *DNA gel electrophoresis for mycoplasma detection in B16F10 cells. The positive control showed a band at approximately 270 bp,*

whereas no corresponding band was detected in the negative control or B16F10 cell sample. The DNA ladder is indicated.

Characterisation of tumour growth

A small-scale pilot experiment was performed to characterise the growth kinetics of subcutaneous B16F10 tumours. Three mice per group were inoculated with either 1×10^5 or 4×10^5 B16F10 cells subcutaneously in the right flank, based on previously reported B16F10 tumour models (Lee, Fujiwara et al. 2015, Shields, Koss et al. 2019). Tumour volumes were measured using callipers over time.

As shown in **Figure 22**, both inoculation doses were sufficient to establish palpable tumours, and tumour growth accelerated markedly at later time points. The tumour growth profile of B16F10 was subsequently considered when designing the treatment schedule for the therapeutic study. Notably, considerable within-group variation in tumour growth was observed, particularly during the later stages of tumour development. This variation may reflect differences between individual animals and technical variation associated with tumour inoculation, highlighting the need for larger group sizes to improve the robustness of subsequent evaluations.

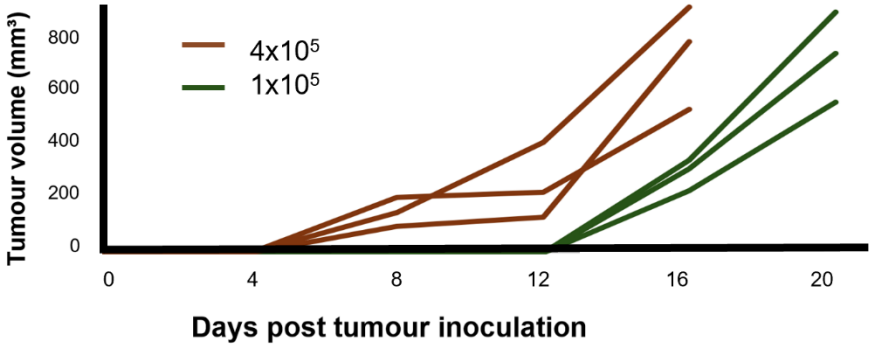


Figure 22. Tumour growth curves of individual mice following inoculation with 4 × 10⁵ or 1 × 10⁵ B16F10 cells. *Each group contained three mice. The 4 × 10⁵ and 1 × 10⁵ cell groups are represented by brown and green lines, respectively.*

3.2.3 Therapeutic efficacy of ROP-mSVN vaccination combined with FLASH radiotherapy

Following validation of both the ROP-mSVN vaccine and the B16F10 tumour model, the therapeutic efficacy of ROP-mSVN vaccination in combination with radiotherapy was evaluated in tumour-bearing mice. To minimise animal use in accordance with the Reduction principle of the 3Rs, a single radiotherapy modality was selected for this initial in vivo study. Based on earlier observations that conventional RT and FLASH RT induced comparable upregulation of survivin (**Figure 1**), FLASH RT was selected given its potential to provide additional immune-sparing benefits (Section 1.2.2).

Experimental design

1×10^5 B16F10 cells were subcutaneously inoculated into C57BL/6 mice on Day 0. Mice were subsequently randomised into four treatment groups receiving adjuvant alone, ROP-mSVN vaccination alone, FLASH radiotherapy alone, or the combination of ROP-mSVN vaccination and FLASH radiotherapy (n = 8).

As vaccination and radiotherapy follow different treatment schedules, establishing an appropriate combination treatment schedule was an important consideration. A sufficient interval between vaccine administrations is generally required to allow the immune response to develop (Da Silva, Martinez et al. 2022). Accordingly, ROP-mSVN was administered on Days 5, 15 and 20 to accommodate the growth window of the B16F10 model. In parallel, a single 10 Gy dose of FLASH radiotherapy was delivered on Day 14, when the B16F10 tumours were expected to have reached approximately 100 mm^3 based on the preliminary tumour growth kinetics (**Figure 22**).

The experimental schedule of combined therapy is illustrated in **Figure 23**. Tumour growth was monitored throughout the study, and the experiment was terminated when most mice in a group developed tumours approaching the predefined ethical size limit of 1000 mm^3.

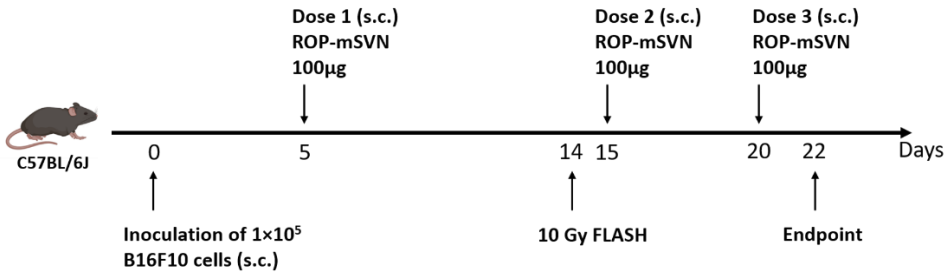


Figure 23. Experimental schedule for ROP-mSVN vaccination combined with FLASH radiotherapy. *C57BL/6J mice were inoculated subcutaneously (s.c.) with 1 × 10^5 B16F10 cells, followed by three doses of 100 µg ROP-mSVN on days 5, 15 and 20. A single 10 Gy dose of FLASH radiotherapy was administered on day 14. Mice were monitored until the experiment was terminated when most mice in a group developed tumours approaching the predefined ethical size limit.*

Tumour growth following treatment

Tumour growth curves for the four treatment groups are shown in **Figure 24**. In the B16F10 model, FLASH radiotherapy alone produced a limited effect on tumour growth compared with the adjuvant control group. In contrast, a delay in tumour growth was observed following ROP-mSVN vaccination, particularly at early stages of tumour development. Notably, the combination of ROP-mSVN vaccination and FLASH radiotherapy resulted in the lowest overall tumour burden among the four treatment groups. However, the difference between the combination and ROP-mSVN monotherapy groups did not reach statistical significance in the overall analysis. The consistently lower tumour burden observed in the combination group suggested a potential therapeutic benefit, but

the present data did not establish a definitive therapeutic advantage, which warranted further investigation.

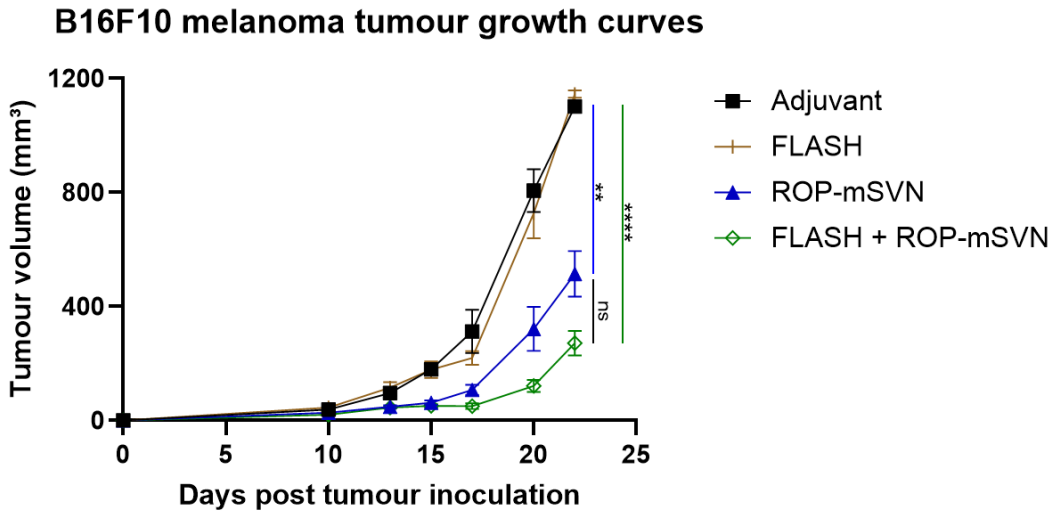


Figure 24. Tumour growth in B16F10 melanoma-bearing mice following treatment. *Tumour growth curves of B16F10 melanoma-bearing mice following different treatments. Data are presented as mean ± SEM. Tumour growth was analysed using a mixed-effects model (REML) with Tukey's multiple comparisons test. The initial group size was n = 8 per group. Group sizes decreased at later time points due to humane endpoints. **P < 0.01, ****P < 0.0001, ns, not significant.*

Of note, the first ROP-mSVN vaccine appeared to have already influenced tumour growth in the combination treatment group before FLASH radiotherapy was administered.

On Day 13, immediately before FLASH radiotherapy, the mean tumour volume was 115.4 ± 18.6 mm³ in the FLASH groups and 45.3 ± 2.5 mm³ in the combined treatment groups, suggesting that tumour growth had already been delayed following ROP-mSVN

vaccination. This pre-existing difference in tumour burden should be carefully considered when interpreting the subsequent response to combination treatment, as differences in tumour size at the time of irradiation may have influenced the response to FLASH radiotherapy and contributed to the subsequent differences in tumour growth between the groups. Alternative treatment sequences should be considered in future studies, including administration of FLASH radiotherapy before vaccination.

Endpoint tumour burden

When tumour burden in the adjuvant control group approached the predefined ethical endpoint, all remaining animals were euthanised and the tumours were collected to enable direct comparison of tumour size at the same time point. Excised B16F10 tumours from all four groups are shown in **Figure 25**. Tumours that were collected before Day 22 are indicated by dashed boxes, while animals euthanised earlier due to tumour ulceration are indicated by circles.

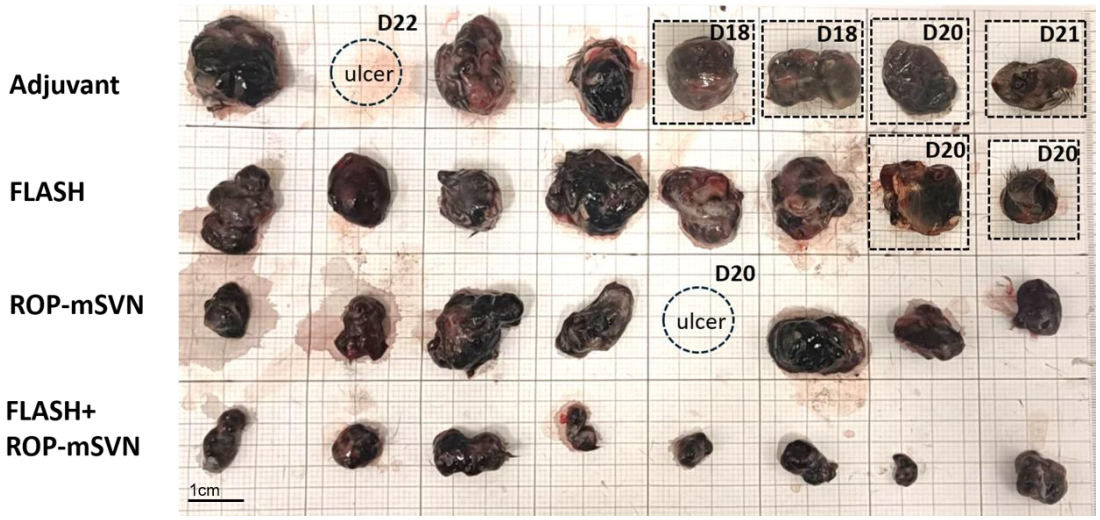


Figure 25. B16F10 melanoma tumours collected at endpoint. *Excised B16F10 melanoma tumours from each treatment group at endpoint. Tumours were collected on day 22 or earlier if humane endpoints were reached. Dashed boxes indicate tumours collected before day 22, and circles indicate animals euthanised due to tumour ulceration.*

Notably, tumour burdens in both the ROP-mSVN monotherapy and combination groups remained relatively low at the study endpoint, which suggests that extending the observation period may be informative in determining whether the lower tumour burden observed in both groups is sustained over time or followed by subsequent tumour progression.

4 Discussion

This study investigated the therapeutic potential of combining a recombinant overlapping peptide-based mouse survivin vaccine, ROP-mSVN, with FLASH radiotherapy in the B16F10 melanoma model. ROP-mSVN was successfully produced using an E. coli-based expression system and subsequently purified by cobalt affinity chromatography. The purified protein exhibited the expected molecular size and was recognised by a survivin-specific monoclonal antibody, supporting its identity as the intended recombinant product. In a preliminary immunogenicity study, ROP-mSVN vaccination induced both humoral and cellular immune responses, although substantial inter-animal variability and the small sample size limited the strength of comparisons. Building on these findings, the therapeutic activity of ROP-mSVN vaccination in combination with FLASH radiotherapy was evaluated in tumour-bearing mice. The combination group showed the lowest tumour burden among the treatment groups, although this difference did not reach statistical significance. These findings therefore provide preliminary evidence for a potential therapeutic benefit of combining ROP-mSVN vaccination with FLASH radiotherapy, while highlighting the need for larger studies with longer follow-up and more comprehensive assessment of tumour response.

4.1 Production of the ROP-mSVN vaccine

The first objective of this study was to produce recombinant ROP-mSVN for subsequent in vivo evaluation. Following IPTG induction under the optimised expression conditions,

a prominent protein band was observed at approximately 33 kDa, consistent with the predicted molecular size of recombinant ROP-mSVN and distinct from the approximately 17 kDa molecular size of WT-mSVN (**Figure 7**), indicating successful expression of the recombinant construct. Subsequent affinity chromatography substantially increased the relative purity of the target protein (**Figure 12**). The purified protein was recognised by a survivin-specific monoclonal antibody (**Figure 13**), providing further evidence of the identity of the recombinant protein.

Insoluble expression of ROP-mSVN

These findings are consistent with previous studies demonstrating that recombinant survivin can be produced in E. coli while retaining its antigenic properties (Zhang, Zhou et al. 2023). A notable feature of the expression profile was the predominance of ROP-mSVN in the insoluble fraction (**Figure 7**). This observation is consistent with previous reports that recombinant proteins expressed at high levels in E. coli frequently accumulate as inclusion bodies (Palmer and Wingfield 2012). Rapid synthesis of a heterologous protein can exceed the folding capacity of the bacterial cytoplasm, promoting intermolecular interactions and aggregation. The relatively large and structurally complex nature of ROP-mSVN may further contribute to this behaviour.

Although lower induction temperatures and reduced IPTG concentrations are commonly used to decrease the rate of recombinant protein synthesis and promote protein solubility

(Francis and Page 2010), these adjustments did not result in more favourable expression of ROP-mSVN in this study (**Figure 5**). The optimal expression conditions therefore depend on the intrinsic properties of the recombinant construct and its interaction with the bacterial expression system.

Double-Band Pattern of WT-mSVN

Interestingly, the purified WT-mSVN sample displayed two closely spaced bands of similar molecular weight, both of which were detected within the expected molecular-weight region (**Figure 12**) and recognised by an anti-Survivin antibody (**Figure 13**), suggesting that the two bands may represent different forms of WT-mSVN. One possible explanation is the presence of different Survivin isoforms generated through alternative splicing, which has been widely reported for Survivin (Conway, Pollefeyt et al. 2000, Jarrin, Mansergh et al. 2012). However, this mechanism is less likely to explain the two bands observed here, as WT-mSVN was expressed from a recombinant construct in E. coli, where alternative splicing is extremely limited compared with eukaryotic systems (Zhiguo, Wang et al. 2013).

In light of this, limited terminal proteolytic degradation of the recombinant protein was considered as another possible explanation, which may generate a slightly smaller protein species while retaining the Survivin epitope recognised by the antibody. However, the stability experiment did not support this explanation, as the relative intensity of the two

bands remained comparable across samples incubated at 4°C for different durations (**Figure 14**), suggesting that protein degradation was unlikely to be the primary cause of the observed two-band pattern. The observed banding pattern may therefore have arisen from other possible factors, including less well-characterised post-translational processes in E. coli, although further investigation would be required to clarify this. Mass spectrometry-based peptide mapping may also help confirm the identity of the two bands.

Considerations for Animal Model Selection

In this study, a mouse survivin-based ROP vaccine, rather than a human survivin-based vaccine that has entered clinical trials, was selected for evaluation of the combination therapy. This allowed the combination therapy to be evaluated in a syngeneic tumour model, thereby preserving the physiological interactions between tumour cells and the host immune system (Carretta, Thorseth et al. 2024).

A more commonly used approach for evaluating vaccines targeting human tumour antigens in mice is to establish tumour cell lines expressing the corresponding human antigen (Zhang, Zhou et al. 2023). This allows direct evaluation of the human survivin-based vaccine used in clinical trials, providing greater clinical relevance. However, the introduction of a foreign human antigen may alter the immunogenicity of mouse tumour cells and their interactions with the host immune system (Brown, Fisher et al. 2001, Yang, Liu et al. 2016). In addition, forced expression of human survivin in tumour cells could be

particularly relevant to the interpretation of the present study, as survivin expression has been associated with responses to both radiotherapy (Section 1.4.3) and ROP-survivin vaccination (Section 1.4.4). The mouse survivin-based approach was therefore selected to enable a more physiologically relevant assessment of tumour responses to the combined therapy.

Nevertheless, this approach also has an important limitation. Although mouse and human survivin share a high degree of sequence identity, the mouse survivin-based vaccine is not identical to OVM-200, and the findings obtained in this study therefore cannot be assumed to fully reflect the therapeutic effects of the human vaccine. Further studies using human survivin-targeting vaccines will be needed to assess whether the combination with FLASH radiotherapy can be translated to the clinical vaccine. Emerging models such as tumour organoids and other human tumour models may provide complementary approaches for investigating this combination in a more clinically relevant setting (Wang, Li et al. 2022).

4.2 Evaluation of ROP-mSVN combined with FLASH radiotherapy

Immunogenicity of ROP-mSVN

Following production and purification of ROP-mSVN, a preliminary immunogenicity study was performed before evaluating the combination therapy in tumour-bearing mice. ROP-mSVN vaccination induced detectable humoral and cellular immune responses

(**Figure 17**, **Figure 18**), providing initial evidence that the recombinant protein was immunogenic in vivo.

Specifically, the 100 μg group reached a higher maximum antibody titre than the 50 μg group (**Figure 17**), suggesting a potentially stronger humoral response at the higher dose. However, variability within groups and the small sample size limited the robustness of comparisons between the two doses. These findings should therefore be regarded as evidence of vaccine immunogenicity rather than definitive evidence for a dose-response relationship.

Therapeutic Efficacy of the Combination therapy

Building on these immunogenicity findings, the therapeutic efficacy of ROP-mSVN vaccination combined with FLASH radiotherapy was subsequently assessed in tumour-bearing mice. In the melanoma B16F10 model, the combination treatment significantly reduced tumour burden compared with the adjuvant control, resulting in the lowest tumour burden among the treatment groups, although the difference between the combination treatment and ROP-mSVN vaccination alone did not reach statistical significance (**Figure 24**).

Therefore, the consistently lower tumour burden observed in the combination group suggested a potential therapeutic benefit of the combination but did not establish a definitive therapeutic advantage.

Notably, tumour burdens in both the ROP-mSVN monotherapy and combination groups remained relatively low at the study endpoint, when tumours in the control group had approached the predefined ethical limit (**Figure 24, Figure 25**). This suggests that extending the observation period may be informative in determining whether the lower tumour burden observed in both groups is sustained over time or followed by subsequent tumour progression. Therefore, following animals individually until they reach their predefined tumour endpoint, rather than terminating all animals when the first group reaches this endpoint, may provide additional information on the therapeutic efficacy of the combined treatment.

FLASH Radiotherapy in the B16F10 Tumour Model

In addition to the combination treatment, the tumour growth curves indicated that 10 Gy FLASH radiotherapy alone provided limited tumour control in the B16F10 melanoma model, with tumour growth remaining broadly comparable to that observed in the adjuvant control group (**Figure 24**). This finding is consistent with previous studies reporting the resistance of B16 melanoma to radiotherapy (Nomura, Abe et al. 2021, Lambing, Tan et al. 2023). The radioresistance of melanoma has been attributed to several factors, including

enhanced DNA damage repair (Wu, Hu et al. 2016), a hypoxic tumour microenvironment (Chavaudra, Guichard et al. 1981), and the presence of radioresistant tumour cell populations (Matchuk, Zamulaeva et al. 2013).

Notably, microbeam radiation therapy (MRT), a novel form of spatially fractionated radiotherapy, has been shown to overcome radioresistance and enhance tumour control in melanoma, including B16F10 models, potentially through an antitumour abscopal effect (Trappetti, Fazzari et al. 2021). Given the limited tumour control achieved with FLASH radiotherapy alone in the present study, combining ROP-mSVN vaccination with alternative radiotherapy approaches, such as MRT, may represent an interesting direction for further investigation.

ROP-mSVN Vaccination in the B16F10 Tumour Model

ROP-mSVN vaccination, either as monotherapy or in combination with FLASH radiotherapy, produced significant tumour suppression compared with the adjuvant control group (**Figure 24**), supporting the antitumour effect of ROP-mSVN in the B16F10 melanoma model. However, tumour growth in both the ROP-mSVN monotherapy group and combination group showed an increasing trend at the later stage of the study, suggesting that the third vaccine dose may have provided limited additional benefit in maintaining tumour control. This may reflect the time required for the protein vaccine to undergo antigen processing and presentation, followed by the activation and expansion of

tumour-specific T cells, before an effective antitumour immune response can be established (Ren, Xiong et al. 2024). As the B16F10 tumours continued to grow rapidly during the later stage of the study, this relatively short interval may have limited the extent to which the immune response induced by the third vaccination could contribute to sustained tumour control. Indeed, maintaining effective tumour control over time remains a challenge in therapeutic cancer vaccination (Zaidi, Jaffee et al. 2025). Several factors may contribute to resistance to cancer vaccines, including an immunosuppressive tumour microenvironment, which can impair effective T-cell function and ultimately promote T-cell exhaustion (Zhou, Wei et al. 2025).

4.3 Limitations and future directions

There are several limitations in the present study that should be acknowledged.

First, while terminating all animals at the same predefined tumour endpoint enabled a direct comparison of tumour burden across treatment groups at the same time point, it resulted in a relatively short follow-up period for the ROP-mSVN-treated groups, limiting the assessment of their longer-term tumour response. In particular, it remained unclear whether the tumour suppression observed in these groups would be sustained or followed by subsequent tumour progression. Extending follow-up by allowing individual animals to be followed until they reach the predefined tumour endpoint could therefore provide a more complete assessment of the therapeutic effect of the combination therapy.

Second, although the treatment schedule was designed to accommodate the required intervals between vaccinations and the tumour size required for irradiation, it may not fully reflect potential clinical treatment sequences. In current clinical practice, radiotherapy is commonly used as part of established treatment, while newer immunotherapeutic approaches are often considered subsequently when standard treatments provide insufficient disease control. Furthermore, in the present study, FLASH radiotherapy was delivered after the first dose of vaccination had already generated a measurable immune response. The resulting difference in tumour size between vaccinated and non-vaccinated groups at the time of irradiation therefore represented an additional factor that may have influenced radiation response and should be considered when interpreting the combination treatment. The tumour growth curves showed that, once established, B16F10 tumours rapidly approached the predefined ethical endpoint (**Figure 22**), which substantially constrained the treatment window available for evaluating different treatment schedules. A tumour model with slower tumour growth may therefore provide more flexibility to examine alternative sequences and intervals between vaccination and radiotherapy.

Third, the preliminary immunogenicity experiment of ROP-mSVN was conducted with a relatively small sample size due to its pilot nature, which limited the robustness of data interpretation. Larger cohorts would be required to confirm the immunogenicity of ROP-

mSVN and to further characterise the relationship between vaccine dose and immune response.

Beyond combining ROP-mSVN with different radiotherapy approaches, additional strategies could be explored to further the antitumor efficacy of combined therapy. For example, the addition of immune checkpoint inhibitors such as anti-PD-1 may help relieve inhibitory signalling within the tumour microenvironment (Park, Im et al. 2026), while strategies that promote T-cell homing to tumours or enhance MHC expression could potentially improve T-cell recruitment and tumour cell recognition (Lanitis, Irving et al. 2025, Darragh and Karam 2026). These approaches may therefore help address immunosuppressive features of the tumour microenvironment and improve the activity of ROP-mSVN-induced immune responses when combined with FLASH-RT.

Future studies may investigate whether the therapeutic effect of the combination with ROP-mSVN is specific to FLASH radiotherapy or can also be achieved with conventional radiotherapy. This would be particularly informative for clinical translation, given that conventional radiotherapy remains a standard treatment for many cancers.

Other radiotherapy approaches could also be explored in combination with ROP-mSVN. As discussed in Section 4.2, MRT, a novel form of spatially fractionated radiotherapy, has been shown to overcome the radioresistance of B16 melanoma (Trappetti, Fazzari et al.

2021). It would therefore be of interest to investigate whether combining ROP-mSVN with MRT or other radiotherapy approaches could further enhance antitumour efficacy.

Finally, as the combination therapy was evaluated in a subcutaneous B16F10 melanoma model in the present study, future studies should extend its evaluation to other tumour settings, including different tumour cell types, orthotopic tumour models and human tumour models. Such studies could help determine whether the observed therapeutic effects are reproducible across different tumour settings and further assess the translational relevance of the combination therapy.

4.4 Conclusion

This study established a recombinant overlapping peptide-based vaccine targeting mouse survivin, ROP-mSVN, which induced both humoral and cellular immune responses in mice. The combination of ROP-mSVN vaccination and FLASH radiotherapy resulted in the lowest tumour burden compared with the adjuvant control and either monotherapy, although further studies are required to confirm its therapeutic potential.

References

Abolfath R, Grosshans D, Mohan R. Oxygen depletion in FLASH ultra-high-dose-rate radiotherapy: a molecular dynamics simulation[J]. Medical Physics, 2020, 47(12): 6551-6561.

Akhunzianov A A, Rozhina E V, Filina Y V, et al. Resistance to radiotherapy in cancer[J]. Diseases, 2025, 13(1): 22.

Anand U, Dey A, Chandel A K S, et al. Cancer chemotherapy and beyond: Current status, drug candidates, associated risks and progress in targeted therapeutics[J]. Genes & Diseases, 2023, 10(4): 1367-1401.

Beltrami E, Plescia J, Wilkinson J C, et al. Acute ablation of survivin uncovers p53-dependent mitotic checkpoint functions and control of mitochondrial apoptosis[J]. Journal of Biological Chemistry, 2004, 279(3): 2077-2084.

Berne A, Petersson K, Tullis I D, et al. Monitoring electron energies during FLASH irradiations[J]. Physics in Medicine & Biology, 2021, 66(4): 045015.

Bolton M A, Lan W, Powers S E, et al. Aurora B kinase exists in a complex with survivin and INCENP and its kinase activity is stimulated by survivin binding and phosphorylation[J]. Molecular Biology of the Cell, 2002, 13(9): 3064-3077.

Bourhis J, Sozzi W J, Jorge P G, et al. Treatment of a first patient with FLASH-radiotherapy[J]. Radiotherapy and Oncology, 2019, 139: 18-22.

Bray F, Laversanne M, Sung H, et al. Global cancer statistics 2022: GLOBOCAN estimates of incidence and mortality worldwide for 36 cancers in 185 countries[J]. CA: A Cancer Journal for Clinicians, 2024, 74(3): 229-263.

Brown D, Fisher T, Wei C, et al. Tumours can act as adjuvants for humoral immunity[J]. Immunology, 2001, 102(4): 486-497.

Cai L, Zhang J, Zhu R, et al. Protective cellular immunity generated by cross-presenting recombinant overlapping peptide proteins[J]. Oncotarget, 2017, 8(44): 76516.

Cao X, Zhang R, Esipova T V, et al. Quantification of oxygen depletion during FLASH irradiation in vitro and in vivo[J]. International Journal of Radiation Oncology Biology Physics, 2021, 111(1): 240-248.

Cao Z, Deng K, Jiang J, et al. Combined treatment of small cell lung cancer using radiotherapy and immunotherapy: Challenges and updates[J]. Biomedicine & Pharmacotherapy, 2025, 182: 117727.

Carmena M, Wheelock M, Funabiki H, et al. The chromosomal passenger complex (CPC): from easy rider to the godfather of mitosis[J]. Nature Reviews Molecular Cell Biology, 2012, 13(12): 789-803.

Carretta M, Thorseth M L, Schina A, et al. Dissecting tumor microenvironment heterogeneity in syngeneic mouse models: insights on cancer-associated fibroblast phenotypes shaped by infiltrating T cells[J]. Frontiers in Immunology, 2024, 14: 1320614.

Chakravarti A, Zhai G G, Zhang M, et al. Survivin enhances radiation resistance in primary human glioblastoma cells via caspase-independent mechanisms[J]. Oncogene, 2004, 23(45): 7494-7506.

Chandra R A, Keane F K, Voncken F E, et al. Contemporary radiotherapy: present and

future[J]. The Lancet, 2021, 398(10295): 171-184.
Chang J, Shin K, Lewis J M, et al. Enhanced Intratumoral Delivery of Immunomodulator Monophosphoryl Lipid A through Hyperbranched Polyglycerol–Coated Biodegradable Nanoparticles[J]. Journal of Investigative Dermatology, 2025, 145(3): 593-604.
Chavaudra N, Guichard M, Malaise E P, et al. Hypoxic fraction and repair of potentially lethal radiation damage in two human melanomas transplanted into nude mice[J]. Radiotherapy and Oncology, 1981, 88(1): 56-68.
Chen L, Yan L, Liu Z, et al. Recent advances in small-molecule radiosensitizers for cancer therapy[J]. Chemical Engineering Journal, 2025, 520: 165858.
Chen X, Duan N, Zhang C, et al. Survivin and tumorigenesis: molecular mechanisms and therapeutic strategies[J]. Journal of Cancer, 2016, 7(3): 314.
Chen X, Nomani A, Patel N, et al. Production of low-expressing recombinant cationic biopolymers with high purity[J]. Protein Expression and Purification, 2017, 134: 11-17.
Cheng B, Ding Z, Hong Y, et al. Research progress in DNA damage response (DDR)-targeting modulators: From hits to clinical candidates[J]. European Journal of Medicinal Chemistry, 2025, 287: 117347.
Coffey J C, Wang J, Smith M, et al. Excisional surgery for cancer cure: therapy at a cost[J]. The Lancet Oncology, 2003, 4(12): 760-768.
Da Silva D M, Martinez E A, Bogaert L, et al. Investigation of the optimal prime boost spacing regimen for a cancer therapeutic vaccine targeting human papillomavirus[J]. Cancers, 2022, 14(17): 4339.
Darragh L B, Karam S D. Radiation as an immune modulator: mechanisms and implications for combination with immunotherapy[J]. Nature Reviews Cancer, 2026, 26(4): 270-284.
Di Y, Meng L, Wang Y, et al. Advances in FLASH radiation therapy: A review on biological foundations and clinical prospects[J]. Translational Oncology, 2026, 65: 102676.
Dohi T, Beltrami E, Wall N R, et al. Mitochondrial survivin inhibits apoptosis and promotes tumorigenesis[J]. The Journal of Clinical Investigation, 2004, 114(8): 1117-1127.
Dong Y C, Nieves L M, Hsu J C, et al. Novel combination treatment for melanoma: FLASH radiotherapy and immunotherapy delivered by a radiopaque and radiation responsive hydrogel[J]. Chemistry of Materials, 2023, 35(22): 9542.
Du C, Fang M, Li Y, et al. Smac, a mitochondrial protein that promotes cytochrome c–dependent caspase activation by eliminating IAP inhibition[J]. Cell, 2000, 102(1): 33-42.
Du J, Kelly A E, Funabiki H, et al. Structural basis for recognition of H3T3ph and Smac/DIABLO N-terminal peptides by human Survivin[J]. Structure, 2012, 20(1): 185-195.
Dunajová L, Cash E, Markus R, et al. The N-terminus of survivin is a mitochondrial-targeting sequence and Src regulator[J]. Journal of Cell Science, 2016, 129(14): 2707-2712.
Durante M, Bräuer-Krisch E, Hill M. Faster and safer? FLASH ultra-high dose rate in radiotherapy[J]. The British Journal of Radiology, 2018, 91(1082): 20170628.
Eggold J T, Chow S, Melemenidis S, et al. Abdominopelvic FLASH irradiation improves PD-1 immune checkpoint inhibition in preclinical models of ovarian cancer[J]. Molecular

Cancer Therapeutics, 2022, 21(2): 371-381.
El Khatib M, Van Slyke A L, Velalopoulou A, et al. Ultrafast tracking of oxygen dynamics during proton FLASH[J]. International Journal of Radiation Oncology, Biology, Physics, 2022, 113(3): 624-634.
Eslami M, Memarsadeghi O, Davarpanah A, et al. Overcoming chemotherapy resistance in metastatic cancer: a comprehensive review[J]. Biomarker Research, 2024, 12(1): 183.
Falleni M, Pellegrini C, Marchetti A, et al. Survivin gene expression in early-stage non-small cell lung cancer[J]. The Journal of Pathology, 2003, 200(5): 620-626.
Fathallah A M, Bankert R B, Balu-Iyer S V. Immunogenicity of subcutaneously administered therapeutic proteins—a mechanistic perspective[J]. The AAPS Journal, 2013, 15(4): 897-900.
Fowlkes N, Clemons K, Rider P J F, et al. Factors affecting growth kinetics and spontaneous metastasis in the B16F10 syngeneic murine melanoma model[J]. Comparative Medicine, 2019, 69(1): 48-54.
Francis D M, Page R. Strategies to optimize protein expression in E. coli[J]. Current Protocols in Protein Science, 2010, 61(1): 5.24.1-5.24.29.
Fu X, Li P, Zhou Q, et al. Mechanism of PARP inhibitor resistance and potential overcoming strategies[J]. Genes & Diseases, 2024, 11(1): 306-320.
Fuller S A, Takahashi M, Hurrell J G. Immunization of mice[J]. Current Protocols in Molecular Biology, 1992, 18(1): 11.14.1-11.14.16.
Galbo P M Jr, Ciesielski M J, Figel S, et al. Circulating CD9+/GFAP+/survivin+ exosomes in malignant glioma patients following survivin vaccination[J]. Oncotarget, 2017, 8(70): 114722.
Garg H, Suri P, Gupta J C, et al. Survivin: a unique target for tumor therapy[J]. Cancer Cell International, 2016, 16(1): 49.
Geetha D, Skaria T. Cathepsin S: a key drug target and signalling hub in immune system diseases[J]. International Immunopharmacology, 2025, 155: 114622.
Geirnaert F, Kerkhove L, Montay-Gruel P, et al. Exploring the metabolic impact of FLASH radiotherapy[J]. Cancers, 2025, 17(1): 133.
Gianfaldoni S, Gianfaldoni R, Wollina U, et al. An overview on radiotherapy: from its history to its current applications in dermatology[J]. Open Access Macedonian Journal of Medical Sciences, 2017, 5(4): 521.
Giannini N, Gadducci G, Fuentes T, et al. Electron FLASH radiotherapy in vivo studies. A systematic review[J]. Frontiers in Oncology, 2024, 14: 1373453.
Grdina D J, Murley J S, Miller R C, et al. A survivin-associated adaptive response in radiation therapy[J]. Cancer Research, 2013, 73(14): 4418-4428.
Gu Y, Yang R, Zhang Y, et al. Molecular mechanisms and therapeutic strategies in overcoming chemotherapy resistance in cancer[J]. Medical Bulletin, 2025, 6(1): 2.
Guo Z, Buonanno M, Harken A, et al. Mitochondrial damage response and fate of normal cells exposed to FLASH irradiation with protons[J]. Radiation Research, 2022, 197(6): 569-582.
Haakensen V D, Öjlert Å K, Thunold S, et al. UV1 telomerase vaccine with ipilimumab

and nivolumab as second line treatment for pleural mesothelioma–A phase II randomised trial[J]. European Journal of Cancer, 2024, 202: 113973.
Haanen J B, Schumacher T N, Kagan J C, et al. Clinical development of cancer vaccines[J]. Nature Medicine, 2026, 32(3): 828-840.
Hartley F, Ebert M, Cook A M J C. Leveraging radiotherapy to improve immunotherapy outcomes: rationale, progress and research priorities[J]. Clinical and Translational Immunology, 2025, 14(4): e70030.
Huang Y, Park Y C, Rich R L, et al. Structural basis of caspase inhibition by XIAP: differential roles of the linker versus the BIR domain[J]. Cell, 2001, 104(5): 781-790.
Huff A L, Jaffee E M, Zaidi N. Messenger RNA vaccines for cancer immunotherapy: progress promotes promise[J]. The Journal of Clinical Investigation, 2022, 132(6).
Ioakeim-Ioannidou M, Rose M, Chen Y L, et al. The use of proton and carbon ion radiation therapy for sarcomas[J]. Seminars in Radiation Oncology, 2024;34(2):207-217.
Jacome A A, Johnson B J C. Minimal residual disease in colorectal cancer: are we finding the needle in a haystack?[J]. Cancers, 2023, 12(7): 1068.
Jansen J, Knoll J, Beyreuther E, et al. Does FLASH deplete oxygen? Experimental evaluation for photons, protons, and carbon ions[J]. Medical Physics, 2021, 48(7): 3982-3990.
Jarrin M, Mansergh F C, Boulton M E, et al. Survivin expression is associated with lens epithelial cell proliferation and fiber cell differentiation[J]. Molecular Vision, 2012, 18: 2758.
Jiang S, Morris T, Forster M D, et al. Phase Ib evaluation of a recombinant overlapping peptide survivin immunotherapy: Safety, immunogenicity, and immune–clinical associations in advanced solid tumours[C]. American Society of Clinical Oncology, 2026: 2651-2651.
Jiang S, Song R, Popov S, et al. Overlapping synthetic peptides as vaccines[J]. Vaccine, 2006, 24(37-39): 6356-6365.
Jin J Y, Gu A, Wang W, et al. Ultra-high dose rate effect on circulating immune cells: A potential mechanism for FLASH effect?[J]. Radiotherapy and Oncology, 2020, 149: 55-62.
Kallinteris N L, Wu S, Lu X, et al. Enhanced CD4+ T-cell response in DR4-transgenic mice to a hybrid peptide linking the Ii-Key segment of the invariant chain to the melanoma gp100 (48-58) MHC class II epitope[J]. Journal of Immunotherapy, 2005, 28(4): 352-358.
Kantoff P W, Higano C S, Shore N D, et al. Sipuleucel-T immunotherapy for castration-resistant prostate cancer[J]. New England Journal of Medicine, 2010, 363(5): 411-422.
Kelly A E, Ghenoiu C, Xue J Z, et al. Survivin reads phosphorylated histone H3 threonine 3 to activate the mitotic kinase Aurora B[J]. Science, 2010, 330(6001): 235-239.
Kersemans V, Gilchrist S, Allen P D, et al. A system-agnostic, adaptable and extensible animal support cradle system for cardio-respiratory-synchronised, and other, multi-modal imaging of small animals[J]. Technology in Cancer Research & Treatment, 2021, 7(1): 39-54.
Khan S, Jutzy J M, Aspe J R, et al. Survivin is released from cancer cells via exosomes[J].

Apoptosis, 2011, 16(1): 1-12.
Khleif S N, Gupta S. Cancer vaccines as enablers of immunotherapy[J]. Nature Immunology, 2025, 26(11): 1877-1889.
Kim J S, Kim H J. FLASH radiotherapy: bridging revolutionary mechanisms and clinical frontiers in cancer treatment–a narrative review[J]. Translational and Experimental Medicine Journal, 2024, 47(4): e54.
Kim M M, Zou W J. Ultra-high dose rate FLASH radiation therapy for cancer[J]. Medical Physics, 2023, 50: 58-61.
Kim Y E, Gwak S H, Hong B J, et al. Effects of ultra-high doserate FLASH irradiation on the tumor microenvironment in Lewis lung carcinoma: role of myosin light chain[J]. International Journal of Radiation Oncology, Biology, Physics, 2021, 109(5): 1440-1453.
Klein C, Brinkmann U, Reichert J M, et al. The present and future of bispecific antibodies for cancer therapy[J]. Nature Reviews Drug Discovery, 2024, 23(4): 301-319.
Knight B B, Oprea-Ilies G M, Nagalingam A, et al. Survivin upregulation, dependent on leptin–EGFR–Notch1 axis, is essential for leptin-induced migration of breast carcinoma cells[J]. Endocrine-Related Cancer, 2011, 18(4): 413-428.
Kochenderfer J, Gress R. A comparison and critical analysis of preclinical anticancer vaccination strategies[J]. Experimental Biology and Medicine, 2007, 232(9): 1130-1141.
Korsemová Ľ, Rybecká S, Levarski Z, et al. Comparison of simple expression procedures in novel expression host Vibrio natriegens and established Escherichia coli system[J]. Journal of Biotechnology, 2020, 321: 57-67.
Kwong F, Hassanzadeh C. Hypofractionated Particle Therapy: A Review of Clinical Data and Implications[J]. The Cancer Journal, 2026, 32(2): e0819.
Labarbe R, Hotoiu L, Barbier J, et al. A physicochemical model of reaction kinetics supports peroxyl radical recombination as the main determinant of the FLASH effect[J]. Radiotherapy and Oncology, 2020, 153: 303-310.
Lambing S, Tan Y P, Vasileiadou P, et al. RIG-I immunotherapy overcomes radioresistance in p53-positive malignant melanoma[J]. J Immunother Cancer, 2023, 15(1): mjad001.
Lanitis E, Irving M, Coukos G. Tumour-associated vasculature in T cell homing and immunity: opportunities for cancer therapy[J]. Nat Rev Immunol, 2025, 25(11): 831-846.
Lee S C, Fujiwara Y, Liu J, et al. Autotaxin and LPA1 and LPA5 receptors exert disparate functions in tumor cells versus the host tissue microenvironment in melanoma invasion and metastasis[J]. Mol Cancer Res, 2015, 13(1): 174-185.
Lee Y T, Tan Y J, Oon C E. Molecular targeted therapy: Treating cancer with specificity[J]. Eur J Pharmacol, 2018, 834: 188-196.
Lens S M, Wolthuis R M, Klompmaker R, et al. Survivin is required for a sustained spindle checkpoint arrest in response to lack of tension[J]. EMBO J, 2003, 22(12): 2934-2947.
Letai A, de The H. Conventional chemotherapy: millions of cures, unresolved therapeutic index[J]. Nat Rev Cancer, 2025, 25(3): 209-218.
Li C F, Wang Y, Li X Y, et al. Improved radiotherapy by survivin small hairpin RNA trigger apoptosis of human lung adenocarcinoma via caspase-3 upregulation in vitro and in vivo[J]. Braz J Med Biol Res, 2017, 28(11): 4812-4818.

Li F, Ackermann E J, Bennett C F, et al. Pleiotropic cell-division defects and apoptosis induced by interference with survivin function[J]. Nat Cell Biol, 1999, 1(8): 461-466.
Li F, Altieri D C. Transcriptional analysis of human survivin gene expression[J]. Biochem J, 1999, 344(2): 305-311.
Li F, Ambrosini G, Chu E Y, et al. Control of apoptosis and mitotic spindle checkpoint by survivin[J]. Nature, 1998, 396(6711): 580-584.
Li Y, Lu W, Yang J, et al. Survivin as a biological biomarker for diagnosis and therapy[J]. Expert Opin Opin Biol Ther, 2021, 21(11): 1429-1441.
Liu J L, Gao W, Kang Q M, et al. Prognostic value of survivin in patients with gastric cancer: a systematic review with meta-analysis[J]. PLoS One, 2013, 8(8): e71930.
Liu Q, Wu P, Lei J, et al. Old concepts, new tricks: How peptide vaccines are reshaping cancer immunotherapy?[J]. Int J Biol Macromol, 2024, 279: 135541.
Luo J, Zhang X J. Challenges and innovations in CAR-T cell therapy: a comprehensive analysis[J]. Front Immunol, 2024, 14: 1399544.
Lynch C, Pitroda S P, Weichselbaum R R. Radiotherapy, immunity, and immune checkpoint inhibitors[J]. Lancet Oncol, 2024, 25(8): e352-e363.
Markosyan N, Vonderheide R H. Developing neoantigen cancer vaccines: where are we now?[J]. Nature Communications, 2026, 17(1): 9700.
Mascia A E, Daugherty E C, Zhang Y, et al. Proton FLASH radiotherapy for the treatment of symptomatic bone metastases: the FAST-01 nonrandomized trial[J]. JAMA Oncology, 2023, 9(1): 62-69.
Matchuk O, Zamulaeva I, Kovalev O, et al. Radioresistance mechanisms of side population cells in mouse melanoma cell line B16[J]. Cell and Tissue Biology, 2013, 7(6): 556-562.
Mc Neil V, Lee S W. Advancing cancer treatment: A review of immune checkpoint inhibitors and combination strategies[J]. Cancers, 2025, 17(9): 1408.
McKenzie J A, Liu T, Jung J Y, et al. Survivin promotion of melanoma metastasis requires upregulation of α 5 integrin[J]. Cancer Cell, 2013, 34(9): 2137-2144.
Min H Y, Lee H Y. Molecular targeted therapy for anticancer treatment[J]. Experimental & Molecular Medicine, 2022, 54(10): 1670-1694.
Montay-Gruel P, Acharya M M, Gonçalves Jorge P, et al. Hypofractionated FLASH-RT as an effective treatment against glioblastoma that reduces neurocognitive side effects in mice[J]. Clinical Cancer Research, 2021, 27(3): 775-784.
Montay-Gruel P, Corde S, Laissue J A, et al. FLASH radiotherapy with photon beams[J]. Medical Physics, 2022, 49(3): 2055-2067.
Munro P D, Ackers G K, Shearwin K E. Aspects of protein–DNA interactions: a review of quantitative thermodynamic theory for modelling synthetic circuits utilising LacI and CI repressors, IPTG and the reporter gene lacZ[J]. Biophysical Reviews, 2016, 8(4): 331-345.
Nalisa M, Luvhengo T E, Kapewangolo P. Effects of surgery on cancer metastasis: biological mechanisms and perioperative implications[J]. Frontiers in Oncology, 2026, 16: 1796434.
Nan X W, Gong L H, Chen X, et al. Survivin promotes piperlongumine resistance in ovarian cancer[J]. Frontiers in Oncology, 2019, 9: 500929.

Napolitano G, Fasciolo G, Venditti P. Mitochondrial management of reactive oxygen species[J]. Antioxidants, 2021, 10(11): 1824.
Nesteruk K P, Psoroulas S. FLASH irradiation with proton beams: beam characteristics and their implications for beam diagnostics[J]. Applied Sciences, 2021, 11(5): 2170.
Ni H, Reitman Z J, Zou W, et al. FLASH radiation reprograms lipid metabolism and macrophage immunity and sensitizes medulloblastoma to CAR-T cell therapy[J]. Nature Communications, 2025, 6(3): 460-473.
Ning Y, Hanna D L, Zhang W, et al. Cytokeratin-20 and survivin-expressing circulating tumor cells predict survival in metastatic colorectal cancer patients by a combined immunomagnetic qRT-PCR approach[J]. Molecular Cancer Therapeutics, 2015, 14(10): 2401-2408.
Nomura D, Abe R, Tsukimoto M. Involvement of TRPM8 channel in radiation-induced DNA damage repair mechanism contributing to radioresistance of B16 melanoma[J]. Biological & Pharmaceutical Bulletin, 2021, 44(5): 642-652.
Ou X, Gao G, Habaz I A, et al. Mechanisms of resistance to tyrosine kinase inhibitor-targeted therapy and overcoming strategies[J]. MedComm, 2024, 5(9): e694.
Oyarzun P, Kobe B. Computer-aided design of T-cell epitope-based vaccines: addressing population coverage[J]. Immunology and Cell Biology, 2015, 42(5): 313-321.
Pail O, Lin M J, Anagnostou T, et al. Cancer vaccines and the future of immunotherapy[J]. The Lancet, 2025, 406(10499): 189-202.
Palavani L B, de Barros Oliveira L, Reis P A, et al. Efficacy and safety of intraoperative radiotherapy for high-grade gliomas: a systematic review and meta-analysis[J]. Neurosurgical Review, 2024, 47(1): 47.
Palmer I, Wingfield P T. Preparation and extraction of insoluble (inclusion-body) proteins from Escherichia coli[J]. Current Protocols in Protein Science, 2012, 70(1): 6.3.1-6.3.20.
Parisi C, Abdayem P, Tagliamento M, et al. Neoadjuvant immunotherapy strategies for resectable non-small cell lung cancer (NSCLC): Current evidence among special populations and future perspectives[J]. Cancer Treatment Reviews, 2024, 131: 102845.
Park J A, Im J, Hwang S M. Decoding T cell exhaustion in the tumour microenvironment[J]. Experimental & Molecular Medicine, 2026: 1-13.
Park M, Yoon H J, Kang M C, et al. PTK7 regulates radioresistance through nuclear factor-kappa B in esophageal squamous cell carcinoma[J]. Tumor Biology, 2016, 37(10): 14217-14224.
Pavlyukov M S, Antipova N V, Balashova M V, et al. Survivin monomer plays an essential role in apoptosis regulation[J]. Journal of Biological Chemistry, 2011, 286(26): 23296-23307.
Pearson A N, Carmicheal J, Jiang L, et al. Contribution of lipid oxidation and ferroptosis to radiotherapy efficacy[J]. International Journal of Molecular Sciences, 2021, 22(22): 12603.
Pennati M, Folini M, Zaffaroni N. Targeting survivin in cancer therapy[J]. Expert Opinion on Therapeutic Targets, 2008, 12(4): 463-476.
Pérez-Baños A, Gleisner M A, Flores I, et al. Whole tumour cell-based vaccines: tuning

the instruments to orchestrate an optimal antitumour immune response[J]. British Journal of Cancer, 2023, 129(4): 572-585.
Qiao Y, Li J, Shi C, et al. Prognostic value of circulating tumor cells in the peripheral blood of patients with esophageal squamous cell carcinoma[J]. OncoTargets and Therapy, 2017: 1363-1373.
Rama N, Saha T, Shukla S, et al. Improved tumor control through T-cell infiltration modulated by ultra-high dose rate proton FLASH using a clinical pencil beam scanning proton system[J]. International Journal of Radiation Oncology, Biology, Physics, 2019, 105(1): S164-S165.
Ramos A, Sadeghi S, Tabatabaeian H. Battling chemoresistance in cancer: root causes and strategies to uproot them[J]. International Journal of Molecular Sciences, 2021, 22(17): 9451.
Ren D, Xiong S, Ren Y, et al. Advances in therapeutic cancer vaccines: Harnessing immune adjuvants for enhanced efficacy and future perspectives[J]. Cancer Biology & Medicine, 2024, 23: 1833-1843.
Ren W, Hou L, Zhang K, et al. The sparing effect of ultra-high dose rate irradiation on the esophagus[J]. Frontiers in Oncology, 2024, 14: 1442627.
Riggio A I, Varley K E, Welm A L. The lingering mysteries of metastatic recurrence in breast cancer[J]. British Journal of Cancer, 2021, 124(1): 13-26.
Rivadeneira D B, Caino M C, Seo J H, et al. Survivin promotes oxidative phosphorylation, subcellular mitochondrial repositioning, and tumor cell invasion[J]. Science Signaling, 2015, 8(389): ra80.
Rödel F, Hoffmann J, Distel L, et al. Survivin as a radioresistance factor, and prognostic and therapeutic target for radiotherapy in rectal cancer[J]. Cancer Research, 2005, 65(11): 4881-4887.
Rodel F, Sprenger T, Kaina B, et al. Survivin as a prognostic/predictive marker and molecular target in cancer therapy[J]. Current Medicinal Chemistry, 2012, 19(22): 3679-3688.
Rosano G L, Ceccarelli E A. Recombinant protein expression in Escherichia coli: advances and challenges[J]. Frontiers in Microbiology, 2014, 5: 172.
Rosini G, Ciarrocchi E, D'Orsi B. Mechanisms of the FLASH effect: current insights and advances[J]. Frontiers in Cell and Developmental Biology, 2025, 13: 1575678.
Ruan J L, Lee C, Wouters S, et al. Irradiation at ultra-high (FLASH) dose rates reduces acute normal tissue toxicity in the mouse gastrointestinal system[J]. International Journal of Radiation Oncology, Biology, Physics, 2021, 111(5): 1250-1261.
Sadelain M. Chimeric antigen receptors: a paradigm shift in immunotherapy[J]. Annual Review of Cancer Biology, 2017, 1: 447-466.
Saxena M, van der Burg S H, Melief C J, et al. Therapeutic cancer vaccines[J]. Nature Reviews Cancer, 2021, 21(6): 360-378.
Schütz A, Bernhard F, Berrow N, et al. A concise guide to choosing suitable gene expression systems for recombinant protein production[J]. STAR Protocols, 2023, 4(4): 102572.

Sellars M C, Wu C J, Fritsch E F. Cancer vaccines: Building a bridge over troubled waters[J]. Cell, 2022, 185(15): 2770-2788.
Shah B A, Holden J A, Lenzo J C, et al. Multi-disciplinary approaches paving the way for clinically effective peptide vaccines for cancer[J]. npj Vaccines, 2025, 10(1): 68.
Shariati A, Khezrpour A, Shariati F, et al. DNA vaccines as promising immuno-therapeutics against cancer: A new insight[J]. Frontiers in Immunology, 2025, 15: 1498431.
Shi X, Yang Y, Zhang W, et al. FLASH X-ray spares intestinal crypts from pyroptosis initiated by cGAS-STING activation upon radioimmunotherapy[J]. Proceedings of the National Academy of Sciences, 2022, 119(43): e2208506119.
Shields B D, Koss B, Taylor E M, et al. Loss of E-cadherin inhibits CD103 antitumor activity and reduces checkpoint blockade responsiveness in melanoma[J]. Cancer Research, 2019, 79(6): 1113-1123.
Siragusa G, Tomasello L, Giordano C, et al. Survivin (BIRC5): Implications in cancer therapy[J]. Life Sciences, 2024, 350: 122788.
Small S, Keerthivasan G, Huang Z, et al. Overexpression of survivin initiates hematologic malignancies in vivo[J]. Leukemia, 2010, 24(11): 1920-1926.
Smith C E P, Prasad V. Targeted cancer therapies[J]. American Family Physician, 2021, 103(3): 155-163.
Song Z, Yao X, Wu M. Direct interaction between survivin and Smac/DIABLO is essential for the anti-apoptotic activity of survivin during taxol-induced apoptosis[J]. Journal of Biological Chemistry, 2003, 278(25): 23130-23140.
Spitz D R, Buettner G R, Petronek M S, et al. An integrated physico-chemical approach for explaining the differential impact of FLASH versus conventional dose rate irradiation on cancer and normal tissue responses[J]. Radiotherapy and oncology, 2019, 139: 23-27.
Srinivasula S M, Ashwell J D. IAPs: what's in a name?[J]. Molecular cell, 2008, 30(2): 123-135.
Stauber R H, Rabenhorst U, Rekik A, et al. Nucleocytoplasmic shuttling and the biological activity of mouse survivin are regulated by an active nuclear export signal[J]. Traffic, 2006, 7(11): 1461-1472.
Tan J, Zhang Y, Wang J, et al. Redefining surgical oncology: active immune microenvironment modulation beyond tumor resection[J]. International Immunopharmacology, 2026, 177: 116521.
Tan S, Day D, Nicholls S J, et al. Immune checkpoint inhibitor therapy in oncology: current uses and future directions: JACC: CardioOncology state-of-the-art review[J]. JACC: CardioOncology, 2022, 4(5): 579-597.
Tao C, Zhang K, Tao Z, et al. Clinical benefits of intraoperative radiotherapy for the recurrence of centrally located hepatocellular carcinoma with microvascular invasion[J]. Cancer Research, 2024, 7(1): e1928.
Tarhini A A, Eads J R, Moore K N, et al. Neoadjuvant immunotherapy of locoregionally advanced solid tumors[J]. Journal for ImmunoTherapy of Cancer, 2022, 10(8): e005036.
Terasaki Y, Terasaki M, Urushiyama H, et al. Role of survivin in acute lung injury: epithelial cells of mice and humans[J]. Laboratory Investigation, 2013, 93(10): 1147-1163.

Tohme S, Simmons R L, Tsung A. Surgery for cancer: a trigger for metastases[J]. Cancer Research, 2017, 77(7): 1548-1552.
Townley A R, Wheatley S P. Mitochondrial survivin reduces oxidative phosphorylation in cancer cells by inhibiting mitophagy[J]. Journal of Cell Science, 2020, 133(21): jcs247379.
Trappetti V, Fazzari J M, Fernandez-Palomo C, et al. Microbeam radiotherapy—a novel therapeutic approach to overcome radioresistance and enhance anti-tumour response in melanoma[J]. International Journal of Molecular Sciences, 2021, 22(14): 7755.
Tsujikawa T, Crocenzi T, Durham J N, et al. Evaluation of cyclophosphamide/GVAX pancreas followed by listeria-mesothelin (CRS-207) with or without nivolumab in patients with pancreatic cancer[J]. Clinical Cancer Research, 2020, 26(14): 3578-3588.
Vader G, Kauw J J, Medema R H, et al. Survivin mediates targeting of the chromosomal passenger complex to the centromere and midbody[J]. EMBO Reports, 2005, 7(1): 85.
Vaidya J S J. Principles of cancer treatment by radiotherapy[J]. Surgery, 2024, 42(3): 139-149.
Veiga G L D, Silva R D M D, Pereira E C, et al. The role of Survivin as a biomarker and potential prognostic factor for breast cancer[J]. Revista Brasileira de Análises Clínicas, 2019, 65(6): 893-901.
Verderio P, Lecchi M, Ciniselli C M, et al. 3Rs principle and legislative decrees to achieve high standard of animal research[J]. Animals, 2023, 13(2): 277.
Verginadis I I, Citrin D E, Ky B, et al. Radiotherapy toxicities: mechanisms, management, and future directions[J]. The Lancet, 2025, 405(10475): 338-352.
Verhagen A M, Coulson E J, Vaux D L. Inhibitor of apoptosis proteins and their relatives: IAPs and other BIRPs[J]. Genome Biology, 2001, 2(7): reviews3009.1.
Verhagen A M, Ekert P G, Pakusch M, et al. Identification of DIABLO, a mammalian protein that promotes apoptosis by binding to and antagonizing IAP proteins[J]. Cell, 2000, 102(1): 43-53.
Vilaplana-Lopera N, Kim J, Nam G, et al. Tissue-specific iron levels modulate lipid peroxidation and the FLASH radiotherapy effect[J]. Communications Biology, 2025, 16(1): 668.
Volovat S R, Scripcariu D V, Vasilache I A, et al. Oncolytic virotherapy: a new paradigm in cancer immunotherapy[J]. International Journal of Molecular Sciences, 2024, 25(2): 1180.
Vozenin M C, Bourhis J, Durante M. Towards clinical translation of FLASH radiotherapy[J]. Nature Reviews Clinical Oncology, 2022, 19(12): 791-803.
Vozenin M C, Montay-Gruel P, Tsoutsou P, et al. Mechanisms, challenges and opportunities for FLASH radiotherapy in cancer[J]. Nature Reviews Clinical Oncology, 2026, 26(1): 62-75.
Wagle N S, Nogueira L, Devasia T P, et al. Cancer treatment and survivorship statistics, 2025[J]. CA: A Cancer Journal for Clinicians, 2025, 75(4): 308-340.
Waldman A D, Fritz J M, Lenardo M J. A guide to cancer immunotherapy: from T cell basic science to clinical practice[J]. Nature Reviews Immunology, 2020, 20(11): 651-668.
Wang Q, Greene M I. Survivin as a therapeutic target for the treatment of human cancer[J].

International Journal of Cancer, 2024, 16(9): 1705.
Wang Y, Li Y, Sheng Z, et al. Advances of patient-derived organoids in personalized radiotherapy[J]. Frontiers in Oncology, 2022, 12: 888416.
Wang Y, Tang S C. Targeted cancer therapy: a comprehensive review of strategies in drug development[J]. Critical reviews in oncology/hematology, 2026: 105303.
Wang Y M C, Ji P, Hariharan S, et al. Clinical pharmacology approaches to support approval of new routes of administration for therapeutic proteins[J]. Clinical Pharmacology & Therapeutics, 2024, 115(3): 440-451.
Warrier N M, Agarwal P, Kumar P. Emerging importance of survivin in stem cells and cancer: the development of new cancer therapeutics[J]. Stem Cell Research, 2020, 16(5): 828-852.
Wculek S K, Cueto F J, Mujal A M, et al. Dendritic cells in cancer immunology and immunotherapy[J]. Nature Reviews Immunology, 2020, 20(1): 7-24.
Wheatley S P, Altieri D C. Survivin at a glance[J]. Journal of Cell Science, 2019, 132(7): jcs223826.
Wiedemuth R, Klink B, Töpfer K, et al. Survivin safeguards chromosome numbers and protects from aneuploidy independently from p53[J]. Molecular Cancer, 2014, 13(1): 107.
Wijaya W, Morris T, Forster M D, et al. Survivin recombinant overlapping peptide (ROP) vaccine in advanced solid tumours: a first-in-human, multicentre, open-label, phase 1a dose-escalation study[J]. European Journal of Cancer, 2026, 91.
Wilson J D, Hammond E M, Higgins G S, et al. Ultra-high dose rate (FLASH) radiotherapy: Silver bullet or fool's gold?[J]. Frontiers in Oncology, 2020, 9: 496435.
Wu L, Hu Z, Huang Y, et al. Radiation changes the metabolic profiling of melanoma cell line B16[J]. PLoS One, 2016, 11(9): e0162917.
Wu Y, Song Y, Wang R, et al. Molecular mechanisms of tumor resistance to radiotherapy[J]. Molecular Cancer, 2023, 22(1): 96.
Wyld L, Audisio R A, Poston G J. The evolution of cancer surgery and future perspectives[J]. Nature Reviews Clinical Oncology, 2015, 12(2): 115-124.
Xiang Y, Liu X, Wang Y, et al. Mechanisms of resistance to targeted therapy and immunotherapy in non-small cell lung cancer: promising strategies to overcoming challenges[J]. Frontiers in Immunology, 2024, 15: 1366260.
Xiao D, Zhang H, Liu Y, et al. Oncolytic viruses: advanced strategies in cancer therapy[J]. Signal Transduction and Targeted Therapy, 2026, 11(1): 45.
Xu H, Zhang D, Zhang Y, et al. TMTP1-modified nanocarrier boosts cervical cancer immunotherapy by eliciting pyroptosis[J]. Theranostics, 2025, 15(11): 5420.
Xu M, Lu X, Sposato M, et al. Ii-Key/HPV16 E7 hybrid peptide immunotherapy for HPV16+ cancers[J]. Vaccine, 2009, 27(34): 4641-4647.
Xu Y, Fang F, Ludewig G, et al. A mutation found in the promoter region of the human survivin gene is correlated to overexpression of survivin in cancer cells[J]. Cell Cycle, 2004, 23(9): 527-537.
Yang D, Welm A, Bishop J M. Cell division and cell survival in the absence of survivin[J]. Proceedings of the National Academy of Sciences, 2004, 101(42): 15100-15105.

Yang F, Liu S, Liu X, et al. In vivo visualization of tumor antigen-containing microparticles generated in fluorescent-protein-elicited immunity[J]. Theranostics, 2016, 6(9): 1453.
Yao Y, Zhou Y, Liu L, et al. Nanoparticle-based drug delivery in cancer therapy and its role in overcoming drug resistance[J]. Frontiers in Microbiology, 2020, 7: 193.
Yarchoan M, Johnson B A 3rd, Lutz E R, et al. Targeting neoantigens to augment antitumour immunity[J]. Nature Reviews Cancer, 2017, 17(4): 209-222.
Zafar A, Khatoon S, Khan M J, et al. Advancements and limitations in traditional anti-cancer therapies: a comprehensive review of surgery, chemotherapy, radiation therapy, and hormonal therapy[J]. Discover Oncology, 2025, 16(1): 607.
Zahedipour F, Zamani P, Mashreghi M, et al. Nanoliposomal VEGF-R2 peptide vaccine acts as an effective therapeutic vaccine in a murine B16F10 model of melanoma[J]. Cancer Nanomedicine, 2023, 14(1): 62.
Zaidi N, Jaffee E M, Yarchoan M. Recent advances in therapeutic cancer vaccines[J]. Nature Reviews Clinical Oncology, 2025, 25(7): 517-533.
Zhang L Q, Wang J, Jiang F, et al. Prognostic value of survivin in patients with non-small cell lung carcinoma: a systematic review with meta-analysis[J]. PLoS One, 2012, 7(3): e34100.
Zhang M, Coen J J, Suzuki Y, et al. Survivin is a potential mediator of prostate cancer metastasis[J]. International Journal of Radiation Oncology, Biology, Physics, 2010, 78(4): 1095-1103.
Zhang M, Liu C, Tu J, et al. Advances in cancer immunotherapy: historical perspectives, current developments, and future directions[J]. Molecular Cancer, 2025, 24(1): 136.
Zhang Q, Gerweck L E, Cascio E, et al. Proton FLASH effects on mouse skin at different oxygen tensions[J]. Physics in Medicine & Biology, 2023, 68(5): 055010.
Zhang S, Zhang C, Song Y, et al. Prognostic role of survivin in patients with glioma[J]. Medicine, 2018, 97(17): e0571.
Zhang Y, Zhou Y, Gong M, et al. Survivin-Based Recombinant Overlapping Peptides Induce T Lymphocyte Cytotoxicity and Prolong the Survival in In Vivo Melanoma Model[J]. Advanced Therapeutics, 2023, 6(11): 2300253.
Zhiguo E, Wang L, Zhou J. Splicing and alternative splicing in rice and humans[J]. BMB Reports, 2013, 46(9): 439.
Zhou J, Guo X, Chen W, et al. Targeting survivin sensitizes cervical cancer cells to radiation treatment[J]. Bioscience Reports, 2020, 40(1): 130-140.
Zhou L Q, Hu Y, Xiao H J. The prognostic significance of survivin expression in patients with HNSCC: a systematic review and meta-analysis[J]. BMC Cancer, 2021, 21(1): 424.
Zhou Y, Wei Y, Tian X, et al. Cancer vaccines: current status and future directions[J]. Journal of Hematology & Oncology, 2025, 18(1): 18.
Zhu H, Xie D, Wang Y, et al. Comparison of intratumor and local immune response between MV X-ray FLASH and conventional radiotherapies[J]. Cancer Radiotherapy, 2023, 27(2): 138-146.
Zugasti I, Espinosa-Aroca L, Fidyt K, et al. CAR-T cell therapy for cancer: current challenges and future directions[J]. Stem Cell Research & Therapy, 2025, 16(1): 210.